Development of Three-dimensional Spiral Injection Scheme by Using Electron Beam

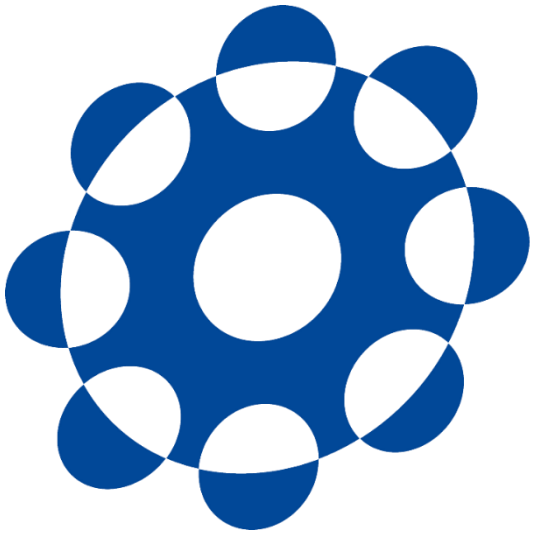

Report of Qualifying

Research in High Energy Accelerator Science

Rehman Muhammad Abdul

ID#20151253

School of High Energy Accelerator Science

Department of Accelerator Science

SOKENDAI

(The Graduate University for Advanced Studies)

Abstract

The muon's anomalous magnetic moment $(g - 2)_\mu$ is one of the most important measurement in elementary particle physics. In order to resolve the current discrepancy between the measurement and the standard model prediction, the J-PARC new muon $g - 2$/EDM (E34) experiment is proposed. The key idea to measure $(g - 2)_\mu$ is to store polarized muon beam in a magnetic field and measure the evolution of spin precession vector. In E34 a very low emittance ultra-cold muon beam of 300 MeV/c from muon accelerator will be stored in a 3-T MRI-type solenoidal magnet within a 0.66-m diameter orbit. A newly developed spiral injection scheme will overcome all technical challenges with small storage orbit. A demonstration experiment to prove the feasibility of this newly proposed scheme is inevitable. Therefore, a scale down Spiral Injection Test Experiment (SITE) by the use of electron beam is under development at KEK Tsukuba campus. The first stage goal of SITE is to detect a DC electron beam spiral track in the storage chamber as fluorescent light from N_2 gas excitation along the electron beam path. The second stage goal is to store the pulsed electron beam for the order of milliseconds.

In the first stage of SITE, DC 80 keV electron beam line of length 2 m has been designed and developed. The electron beam in straight beam line was successfully commissioned and confirmed at several locations by using fluorescent screen (FS) monitors. For further investigation of the straight beam line, a simulation was done in CST-PS. Meanwhile, a solenoidal type storage magnet was manufactured to store electron beam into 24 cm diameter orbit. Simulation of the storage magnet and particle tracking studies has been carried out in CST-PS. Injection of the electron beam in the storage chamber has been performed with several different experimental settings and optimal condition for injection of the electron beam has been determined from this systematic

study. Many other efforts also have been made for the successful injection of the electron beam from the straight beam line into the storage magnet. Finally, the electron beam was successfully injected from straight beam line to the storage magnet and confirmed by using FS monitors. Electron beam of 80 keV in the storage magnet was observed in a non-interceptive way, as fluorescent light due to excitation of nitrogen gas along beam track using a CCD-camera. However, we found one major issue. Due to the radial field of the storage magnet beam was vertically defocused and only two turns were clearly observed. Twiss parameters at the injection point will be controlled in order to solve vertical defocusing of the beam.

For the first stage of SITE experimental setup has been built successfully and goal to observe electron beam as fluorescent light in the storage magnet is achieved. It is figured out that what is needed to be done in order to achieve the second stage goal.

For the second stage of SITE, an electric chopper system has been designed, simulated and fabricated to produce a pulsed electron beam of a pulse length 50 ns. This report will describe the achievements of the first stage of SITE and the progress towards the second stage.

Table of Contents

List of Figures

List of Tables

Acknowledgments

There are so many people I wish to thank who have in one way or another made this report possible. I would like to express my sincere gratitude to my supervisor Prof. Kazuro Furukawa for his constant support, guidance and motivation academically and otherwise. The door to Prof. Kazuro Furukawa office was always open whenever I ran into a trouble spot.

I wish to give special thanks to my Co-supervisor Tsutomu Mibe for his incredible support and encouragement. I am much obliged to him for providing me an opportunity to participate in Muonium Production Experiment at J-PARC, which greatly benefit me for enhancing my experimental expertise. I would like to express my deepest gratitude to Prof. Hiromi Iinuma for her continuous support and providing me an opportunity to study in SOKENDAI. I have been extremely lucky to have her one of my supervisor who cared so much about my work, and who responded to my questions and queries so promptly.

I am much obliged to Prof. Satoshi Ohsawa for his support academically and in my daily life. His teaching and support was indispensable for the completion of this report. I would like to thank Prof. Hisayoshi Nakayama. He has been supportive since the days I began my work at the experiment. I am indebted to Prof. Hiromi Hisamatsu for his kind help during the experiment and for providing us many crucial vacuum component.

I am grateful to Prof. Nahito Saito for giving me many constructive comments and suggestion during weekly meetings. I would also like to thank all saito's lab member: Ryo Kitamura, Masashi Otani, Sirui Li, Yutaro Sato, Hiromasa Yasuda, Shoichiro Nishimura.

Finally, I must express my gratitude to my mother and siblings for their prayers and countless love for me.

Chapter 1

Introduction

Ever since the discovery of muon, physicists are trying to decipher the properties of muons. A precise measurement of muon anomalous magnetic moment property can give hint for new physics beyond the standard model.

The BNL [1] experiment measured the muon's anomalous magnetic moment $(g-2)_\mu$ to an accuracy of 0.54 ppm, and there is ~3 σ discrepancy between the experimental value and the Standard Model prediction. More precise measurement of the muon $(g-2)_\mu$ and its electric dipole moment (EDM) is in preparation at the J-PARC in order to search physics beyond the standard model. The J-PARC new muon $g-2$/EDM (E34) experiment aims to measure $(g-2)_\mu$ to the precision of 0.1 ppm and EDM down to the sensitivity of 10^{-21} e.cm [2].

The E34 experiment will employ a completely different and innovative experimental approach as compared to the previous measurements at CERN and BNL [1, 3] to realize this experiment. The key idea to measure $(g-2)_\mu$ is to store polarized muon beam in the magnetic field and measure the evolution of spin precession vector with respect to time. An ultra-cold muon beam [4, 5] of 300 MeV/c from muon LINAC with very small emittance (1.5π mm mrad) will be injected into the 3-T MRI type superconducting magnet to store muon beam in 0.66 m diameter orbit [6]. A novel three-dimensional spiral injection scheme has been proposed to inject ultra-cold muon beam into such compact storage ring. This newly proposed spiral injection scheme has no real precedent, therefore, it is necessary to prove the feasibility of this injection scheme. This new injection scheme will be establish with an electron beam. Spiral Injection Test Experiment (SITE) is a scale

down demonstration for the establishment of newly proposed injection scheme and under development at KEK LINAC's klystron gallery Tsukuba campus. SITE will provide the freedom to perform the experiment without stringent time constraint of muon beam availability at J-PARC. It is also easier to handle electron beam parameters such as beam energy and current which will provide freedom to choose them according to experiment needs.

SITE is divided into two stages:

1) In the first stage of SITE DC electron gun (80 keV), straight beam line to transport electron beam and normal conducting storage magnet have been prepared and assembled together. Storage magnet for SITE contains all important features as in the original storage magnet. In the first stage, it is decided to observe electron beam as fluorescent light due to introduced nitrogen gas excitation along the beam track. The final goal of the first stage is to observe 80 keV electron beam trajectories of 24 cm diameter as a fluorescence light in the storage magnet 83 gauss field.

2) In the second stage of SITE electric chopper system to produced pulsed electron beam is developed. A magnetic kicker to guide electron beam to the very center of storage region and beam monitors to determine the efficiency of this scheme are also planned to develop in the second stage. The second stage goal is to store the pulsed electron beam for the order of few milliseconds.

Many challenges have to face during the commissioning of the first stage. This report will describe the progress and results from the first stage of SITE. Electric chopper system to produce pulsed beam also has been developed for the second stage and will be described in details.

The organization of this report is as follow. Chapter 2, introduce the need and basic concept of spiral injection scheme briefly. Experimental setup and detail of each component and simulation are also given in Chapter 2. Results from the first stage of SITE, problems and challenges faced during beam commissioning are discussed in chapter 3. Summary and conclusion are given in chapter 4.

Chapter 2

Three-Dimensional Spiral Injection Scheme

One of the key challenge in new g - 2/EDM experiment at J-PARC (E34) is to inject ultra-cold muon beam into a compact and highly uniform magnetic field storage ring. A 3 T MRI-type solenoidal magnet will be used to store muon beam into a diameter of 66 cm orbit. Mid-plane of the solenoidal magnet is defined as the storage region for muon beam with field uniformity of < 1 ppm variation [6]. In this chapter, the necessity for the spiral injection and basic concepts of muon 3-D spiral injection scheme will be described briefly. Spiral Injection Test Experiment (SITE) setup and detail of each component are also given in this chapter.

2.1 The Basic Concept of Muon Injection Scheme

In the previous BNL muon $g - 2$ experiment muon beam of 3.09 GeV/c was injected into a 1.45 T storage ring of radius 7.11 m. A device called an inflector [7] was used to cancel fringe field of storage magnet to prevent deflection of the beam due to a fringe field. To avoid beam hit at the wall of inflector after one turn beam kicked horizontally by the kicker to move the central orbit.

This type of scheme is applicable if the radius of the storage ring is sufficiently large as compared to the thickness of inflector wall. In BNL case radius of the storage ring was 711 cm and the thickness of the inflector wall was 1 cm, hence kick angle of 1.5 mrad was required within 149.2 ns (cyclotron period).

E34 storage magnet strength is 3 T which is too high field to cancel by any device. In E34, the radius of the central beam orbit is only 33 cm using BNL type kicker will need a horizontal kick angle of 30 mrad within 7.4 ns (cyclotron period). 30 mrad kick angle

within 7.4 ns is not possible by using any existent technology. Hence, BNL injection scheme is not applicable in the case of E34.

To overcome these difficulties three-dimensional spiral injection scheme has been developed to inject muon beam into the storage magnet. The basic concept of three-dimensional spiral injection is depicted in Fig. 2.1. Muon beam will be injected at a vertical angle into a 3-T MRI type solenoidal magnet. A carefully designed radial fringe field will convert the vertical component of momentum into horizontal as its approach to the storage region. When muon beam will reach to the storage region a double anti-Helmholtz type kicker will completely remove the vertical component and muons will be stored in mid plane as shown in Fig. 2.2. A weak focusing will be applied to a muon beam in the storage region in order to reduce the requirement of the muon beam "coldness" [6]. Detailed study of this new injection scheme is published in [6].

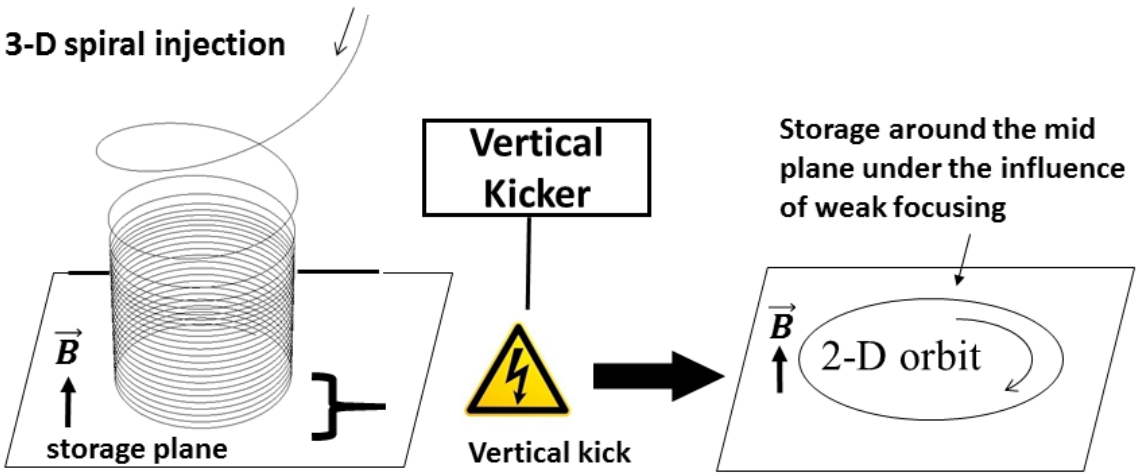

Figure 2.1: The Basic concept of three-dimensional spiral injection scheme [6]

.

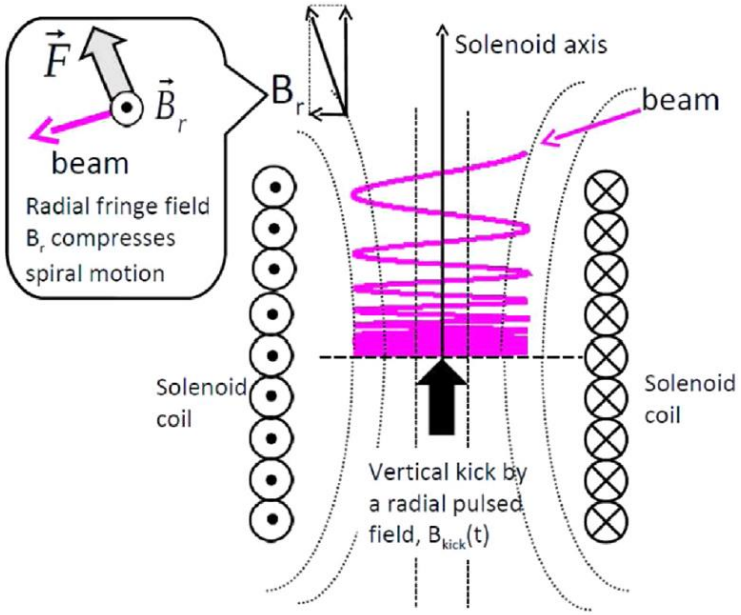

Figure 2.2: Radial field of solenoidal type magnet will deflect vertical momentum of muon beam to the horizontal [6].

It is the first instance to employ the idea of 3-D spiral injection scheme. Therefore, a test experiment to establish the feasibility of this new injection scheme is indispensable. In the next section, detailed experimental setup for the establishment of this new scheme is described in detail.

2.2 Spiral Injection Test Experiment (SITE) by Using Electron Beam

Spiral Injection Test Experiment (SITE) by the use of electron beam is under development for the establishment of spiral injection scheme. As described earlier SITE is divided in to two stages. In the first stage of SITE experimental setup has been prepared, namely electron beam line and storage magnet. In the second stage of SITE, electric chopper system to produced pulsed electron beam has been developed. In this section, experimental setup of SITE has been described in detail.

2.3 Experimental Setup of SITE

A comparison of SITE with E34 is given in Table 2.1. Test experiment is consist of straight beam line and storage magnet, a schematic diagram of the experiment is shown in Fig. 2.3. The straight beam line is 2 m long. At the beginning of straight beam line a DC thermionic electron gun of 80 keV is used to produce an electron beam. A magnetic lens at the distance of 70 mm away from the electron gun serves as a focusing element for the electron beam in the straight section. A collimator of 3 mm diameter and length of 5 mm is placed at 700 mm away from electron gun to control the beam halo in a drift section of straight beam line and also used to maintain the differential vacuum for storage magnet. A dipole magnet on the straight beam line is used to bend electron beam into the storage magnet. To control the transverse position (x - y) of electron beam, five pairs of steering coils have been installed on the straight beam line. Two of them are placed just after magnetic lens. A pair of x–steering coil and y–steering coil are placed before collimator to control the beam transverse position at the collimator. The fifth x-steering coil is placed on the injection pipe after main dipole magnet to control the horizontal

positon of the electron beam. Three fluorescent screen (FS) monitors have been placed to detect transverse profile of the electron beam along beam line. First FS monitor is placed on the collimator and beam profile from this FS monitor has been captured by the use of mirror and digital camera 1. Second FS monitor is placed at the end of beam line and beam profile is captured by CCD-camera 2. Third FS monitor is placed at the injection pipe and seen by CCD-camera 3. The detail setup of FS monitors will be described in chapter 3. The photo of actual experimental setup is shown in Fig. 2.4. The detail of each component is presented in the subsequent sections.

Table 2.1: Comparison of parameters between J-PARC *g* - 2/EDM experiment and test experiment.

Parameters	**E34**	**Test experiment**
Storage magnetic field	3-T	0.0083 T
Particle specie	μ^+	e^-
Momentum	300[MeV/*c*]	0.296 [MeV/*c*]
Cyclotron period	7.4 nsec	5.0 nsec
Storage orbit diameter	0.66 m	0.24 m

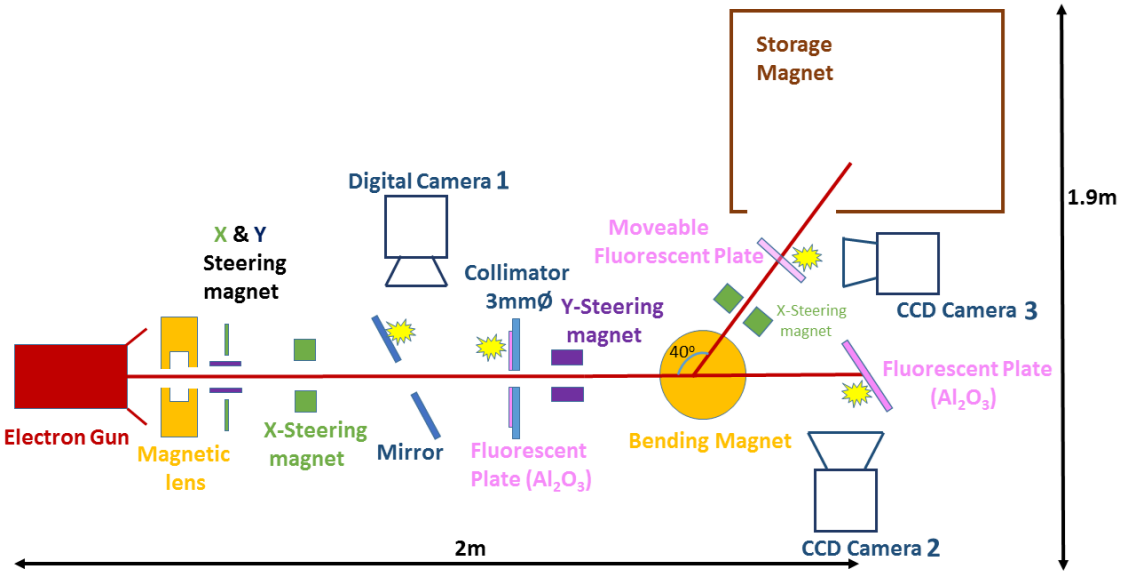

Figure 2.3: Schematic diagram of test experiment.

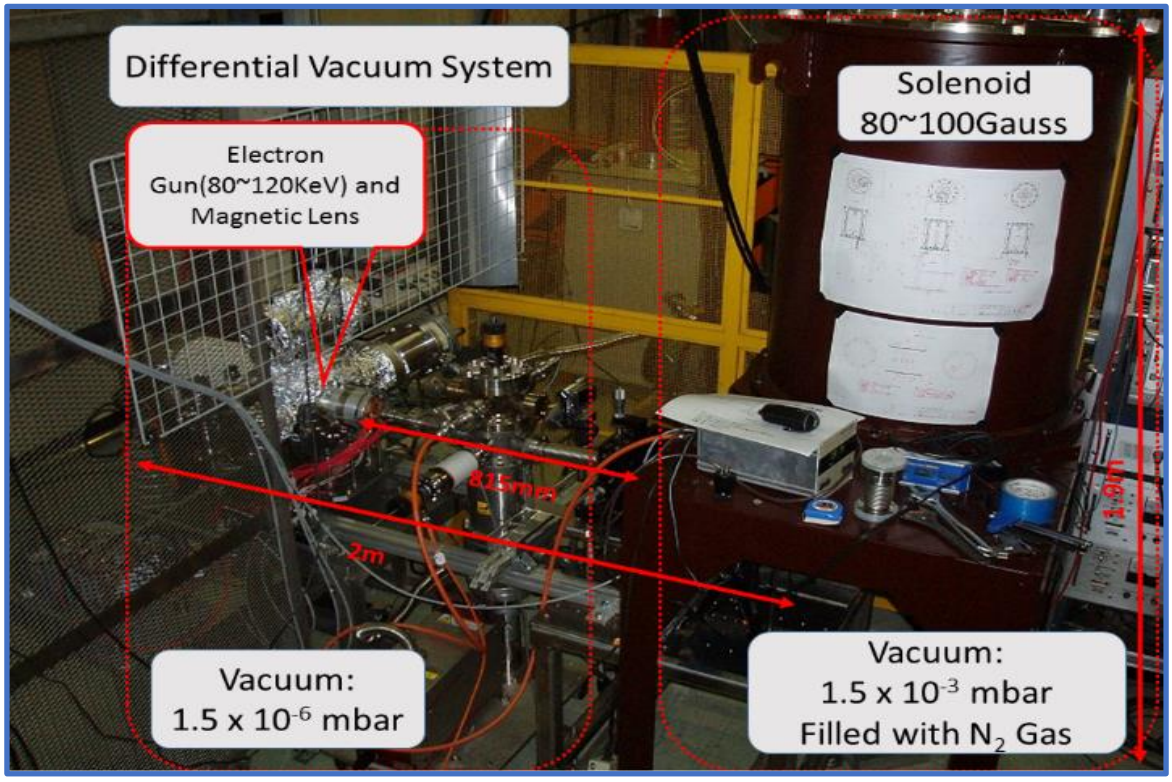

Figure 2.4: Photo of test experiment setup at the KEK-LINAC building.

2.3.1 Electron Gun

A thermionic electron gun with LaB_6 cathode of 2 mm diameter is in use to produce the electron beam. This electron gun was previously used for the production high brightness X-ray experiment [9]. The electron gun is operating at 80 keV and maximum achievable beam current is <100 mA. From radiation and thermal safety point of view, electron gun is in operation at 74 μA. An isolation transformer of 200 kV is used to transfer electrical power from AC source to high voltage power supply of electron gun. Specifications of electron gun are given in Table 2.2. Experimental layout of electron gun H.V power supply is shown in Fig. 2.5.

Table 2.2: Parameters of electron gun.

Parameters	**Value**
Extraction Voltage	80 keV
Maximum current	<100 mA
Grid Type	Aperture
Cathode emission	Thermionic
Cathode material	LaB_6
Cathode Diameter	2.0 mm
Cathode Grid Voltage	2 keV
Emittance	a few mm mrad

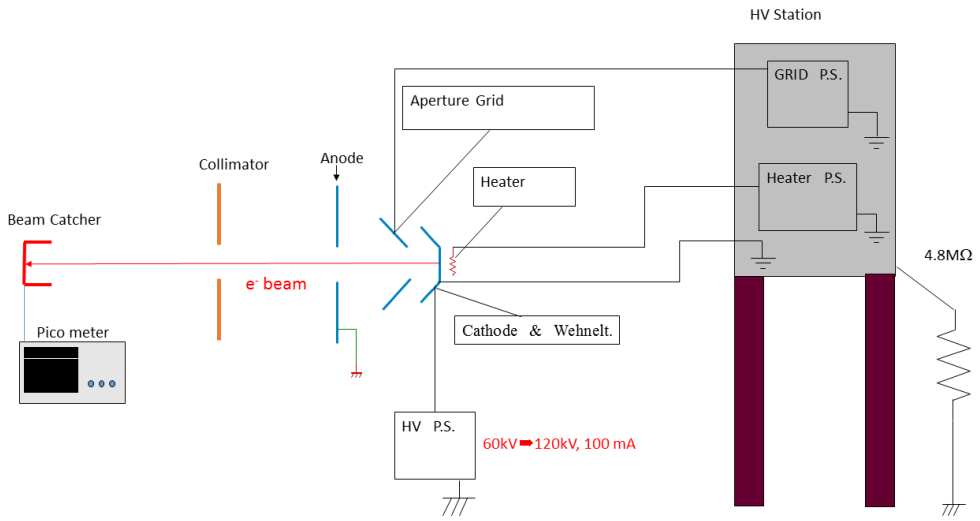

Figure 2.5: Layout of electron gun H.V power supply [9].

Cathode: The low work function (2.70 eV) and high electron yield make LaB_6 one of best candidate material for cathode of electron gun. LaB_6 require modest vacuum and 50 times the service life of tungsten cathode. LaB_6 cathode of diameter 2 mm is used in the electron gun of SITE as shown in Fig. 2.6.

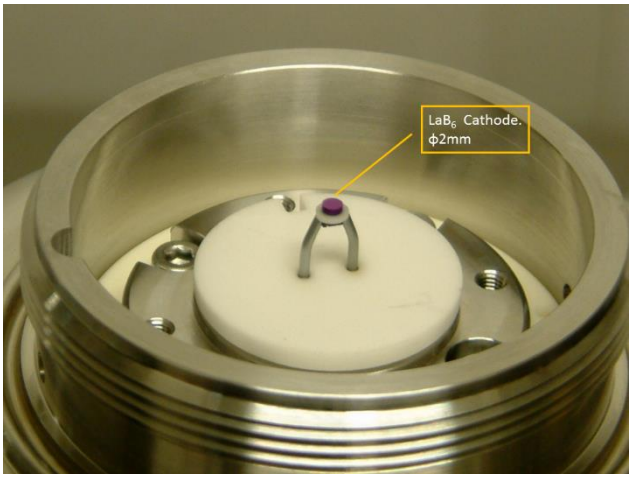

Figure 2.6: LaB_6 cathode used in electron of test experiment [9].

2.3.1.1 Thermionic Emission

When a piece of a metal is heated to very high temperatures, electrons achieve enough energy to overcome the potential barrier and flee away from the metal. The electron

emission subject to thermal excitation is called “thermionic emission”. For the electrons to be free from the metal, need energy at least equal to “potential barrier φ” or “work function” of that particular metal. In other words the energy of an electron after escaping from the metal would be

$$E \geq E_f + \varphi$$

In thermionic emission model, the maximum amount of emitted particles is strongly dependent on the temperature of the surface. The thermionic emission model is principally based on the space-charge limited model in combination with a maximal extractable current. In temperature limited case Richardson's law gives the current density J_x [A/m^2] of emitted electrons

$$J(x) = A_R T^2 \exp\left(\frac{-W}{kT}\right) \tag{2.1}$$

Where A_R is Richardson's constant with a value A_R = 1.2x10^6 A/m^{2}K^2. W is work function the metal. T is applied temperature; k is Boltzmann constant [10 - 11].

In space charge limited case Childs-Langmuir Law gives the current density J_x [A/m^2] of emitted electrons

$$J(x) = \left[\frac{4\epsilon_0}{9}\sqrt{\frac{2e}{m}}\right]\frac{V_A^{3/2}}{b^2} \tag{2.2}$$

Where J_A is current density, V_A applied voltage, ϵ_0 is permittivity of free space, b is the distance from emitting surface, m and e are mass and charge of electron [12].

2.3.1.2 Simulation of Electron Gun

CST PARTICLE STUDIO is an expert tool for the fast and precise study of charged particle dynamics in 3D electric and magnetic fields [13]. Simulation of electron gun has been carried out in CST-PS to study beam dynamics at the exit of electron gun.

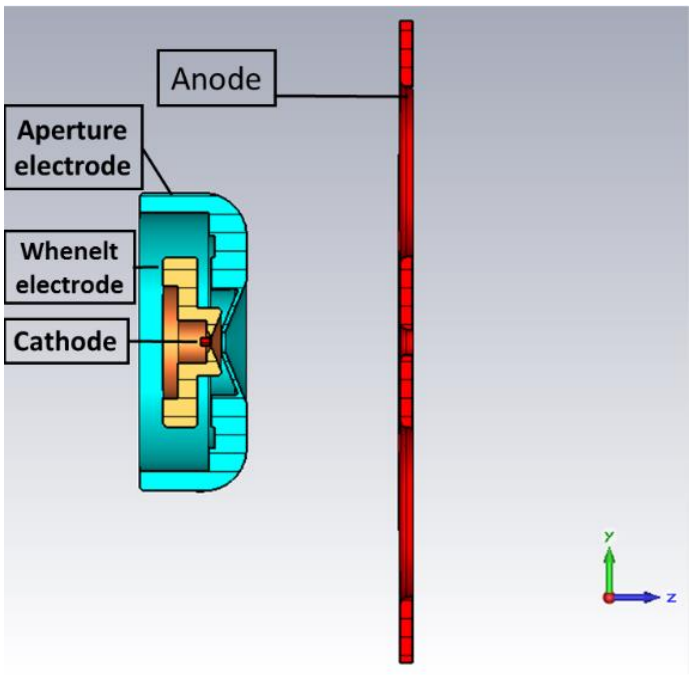

Figure 2.7: Model of electron gun in CST

Figure 2.7 is the 3D model of the electron gun in CST. Figure 2.8 (a) shows potential contours on the electrodes and (b) depicts electric field pattern and strength on gun's electrodes. For a low current application, electron gun has to be operated in temperature limited regime in which cathode temperature (heater current) decide beam current. Thermionic emission model (Richardson's law) has been selected for the particle emission from cathode surface. Maxwell-Boltzmann distribution is chosen for particles (8036) at the surface of the cathode. Beam trajectories at -80 kV cathode potential, aperture voltage 2 kV and temperature of 1250 K are shown in Fig. 2.9. Figure 2.10 is CST-PS simulation result of beam current as a function of cathode temperature. At 900 K, beam current is $2.3 \times 10^{-9}\ A$ which increases up to $52 \times 10^{-3}\ A$ at after 1700 K temperature limited regime reach and cathode temperature has no effect on beam current. In order to increase beam current after this temperature-limited regime we have to increase aperture electrode potential.

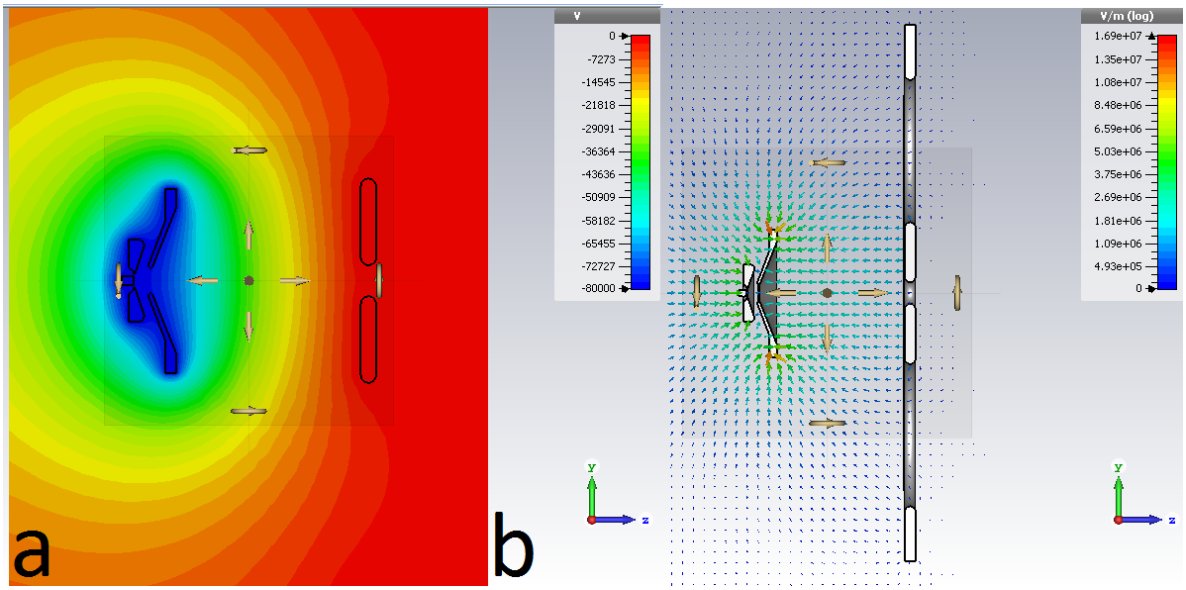

Figure 2.8: (a) Potential contours on the electrodes of electron gun. (b) Electric field pattern and strength among electrodes of electron gun.

In Fig. 2.9 beam waist is visible after aperture electrode this waist also cause beam halo in post anode region. To avoid beam halo a collimator has been used which will be discussed in later section.

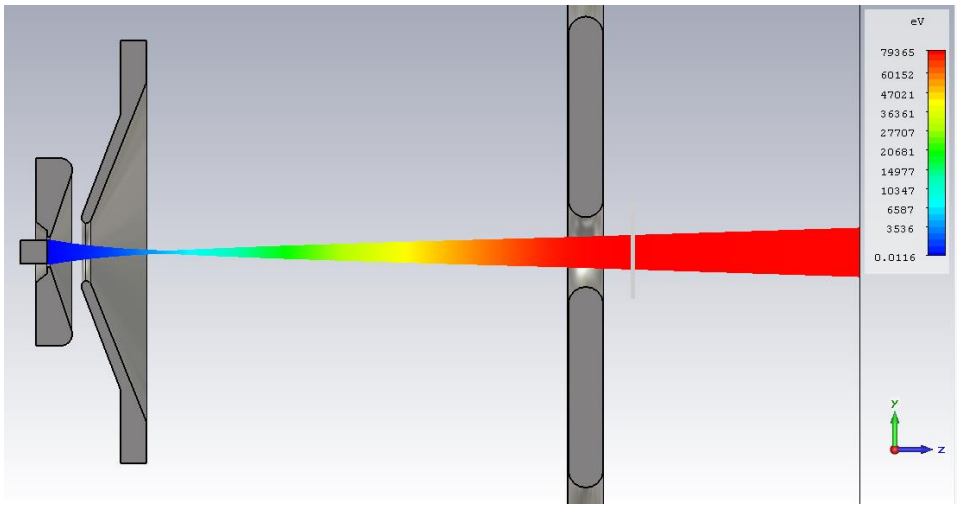

Figure 2.9: Beam trajectories from electron gun at -80 kV cathode potential, 2 kV aperture electrode and cathode temperature of 1250 K.

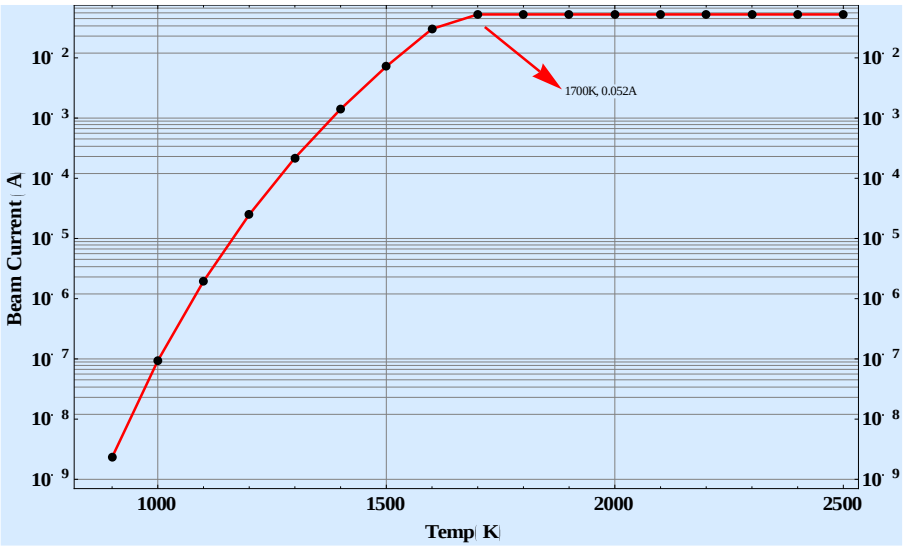

Figure 2.10: Beam current as a function of cathode temperature.

2.3.1.3 Twiss Parameters

To calculate Twiss parameters in post anode region, distribution of 8038 particles from CST-PS have been taken. Figure 2.11 is a transverse (x-y) cross section of a beam at 50 mm away from the cathode. Figure 2.12 and 2.13 are x-phase space distribution and y-phase space distribution respectively.

$$\varepsilon_{rms} = \sqrt{\left\langle \left(x - \langle x \rangle\right)^2 \right\rangle \left\langle \left(x' - \langle x' \rangle\right)^2 \right\rangle - \left\langle \left(x - \langle x \rangle\right)\left(x' - \langle x' \rangle\right) \right\rangle^2} \tag{2.3}$$

$$\beta = \frac{x_{rms}^2}{\varepsilon_{rms}} \tag{2.4}$$

$$\alpha = \frac{(xx')_{rms}}{\varepsilon_{rms}} \tag{2.5}$$

$$\gamma = \frac{x_{rms}'^2}{\varepsilon_{rms}} \tag{2.6}$$

$$\beta\gamma - \alpha^2 = 1 \tag{2.7}$$

Equation 2.3 is the statistical definition of emittance. Equation 2.4 to 2.6 are definition of Twiss parameters, those are used to calculate Twiss parameters at the exit of anode from CST-PS output. Table 2.3 shows the results of these calculations.

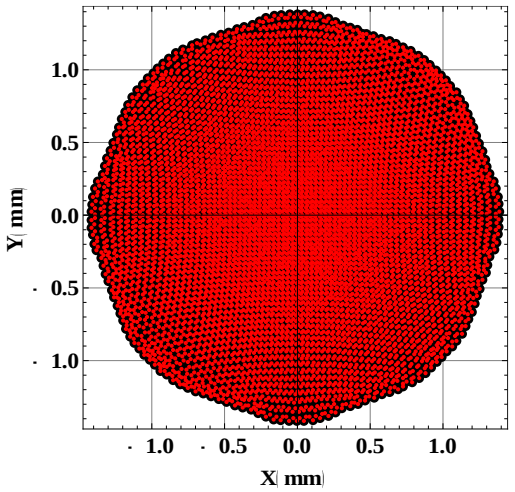

Figure 2.12: x-y cross section of beam in post anode region (50 mm away from cathode surface).

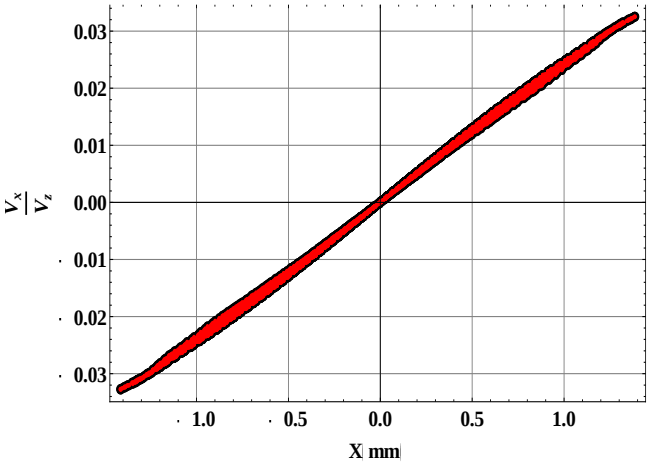

Figure 2.11: x-phase space of particle distribution at the 50 mm away from cathode.

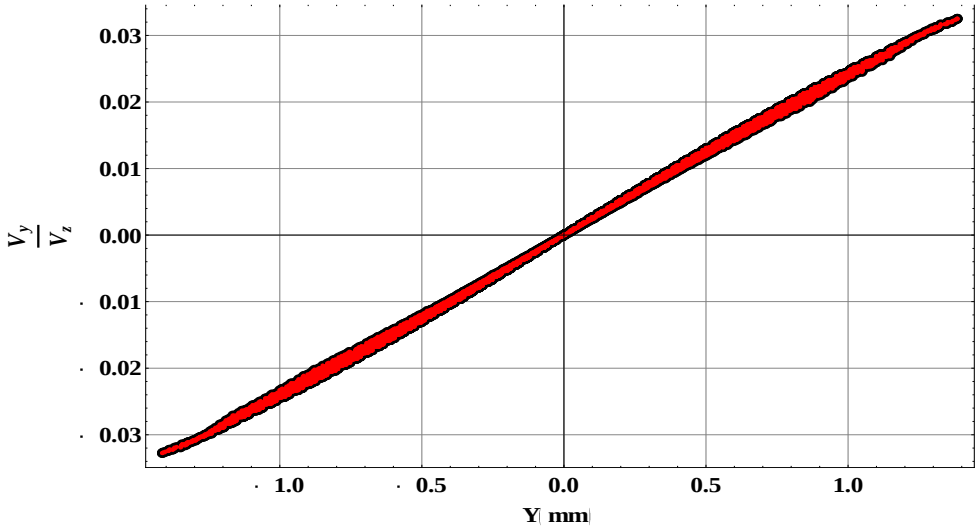

Figure 2.13: y-phase space of particle distribution at the 50 mm away from cathode.

Only simulation study has been carried out for the electron gun, results are not confirmed experimentally yet because our first target was to inject electron beam into the storage magnet. In near future I will confirm these results experimentally.

Table 2.3: Twiss parameters at the exit of anode.

Parameters	Value
$\varepsilon_{rms}(m\ rad)$	3.12×10^{-7}
β	0.098
α	3.37
γ	126.4
$\beta\gamma-\alpha^2$	1

2.3.2 Magnetic Lens

A magnetic lens is used to focus the electron beam after the anode of the electron gun. Magnetic lens is consists of a coil of copper wires inside the iron pole pieces. A current through the coils produces a magnetic field in the bore of the pole pieces. The rotationally symmetric magnetic field is inhomogeneous in such a way that it is weak in the center of the gap and becomes stronger close to the bore. Electrons close to the center are less strongly deflected than those passing the lens far from the axis. The overall effect is that a beam of parallel electrons is focused into a spot.

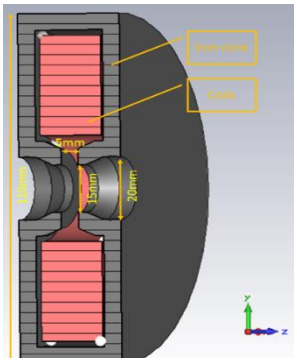

Figure 2.14: Magnetic lens model with its dimensions.

The magnetic lens in test experiment is consists of a single coil with 560 windings and 5 mm thick iron shielding. The magnetic lens length is about 30 mm. Magnetic lens is air-cooled. The magnetic iron cover of solenoid provides a return path for magnetic field screening effectively the field in the outer space and concentrating it inside solenoid gap of 5 mm. Focusing power (reciprocal of focal length) of a magnetic lens is given by the following formula [14]

$$\frac{1}{f_{sol}} = \frac{e^2}{4\gamma^2\beta^2m^2c^2}\int (B_z)^2 dz \tag{2.8}$$

Figure 2.14 is showing the schematic of magnetic lens. Figure 2.15 (a) and (b) are representing absolute value of magnetic absolute and radial component respectively.

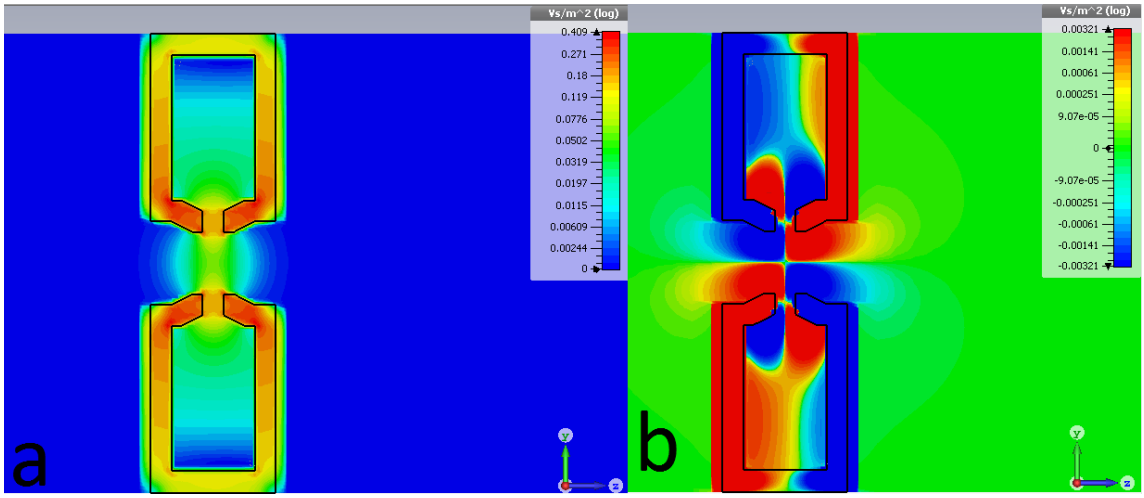

Figure 2.15: (a) Absolute value of magnetic lens. (b) Radial component of magnetic field.

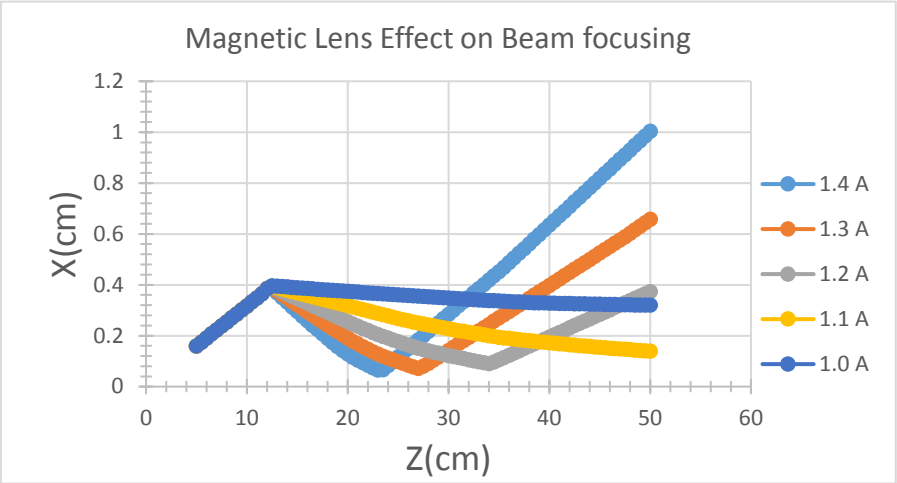

Figure 2.16: Transverse beam size (+x direction) as it is evolving in beam direction. Different colors curves show focusing strength of magnetic lens at different magnetic lens current.

To find the optimal condition for the focusing of the electron beam by the use of the magnetic lens, tracking simulation in CST-PS has been carried out. Figure 2.16 present magnetic lens effect on focusing of the electron beam. Magnetic lens center position is 11 cm in Fig. 2.16. Different colors correspond to different values of magnetic lens current. Collimator position is assumed at 50 cm away from the electron gun. As we change the current of magnetic lens, the focal length of beam change. At current 1 A, beam almost focus at collimator, which means most of the beam will pass through collimator without much dissipation. I performed this simulation study but so far didn't have chance to check these values experimentally due to other more important ongoing studies in the experiment.

2.3.3 Main Dipole Magnet

As a part of SITE, a dipole magnet was designed, fabricated, and tested. The magnet design and geometry are resulted on Ø 46 mm circular poles with a gap of 18 mm and yoke size of 103 mm × 140 mm. In the simulation, linear material with permeability of

5000 was used, which is close to actual material used in magnet fabrication. The magnet consists of two coils with 32 windings each.

Bending radius ρ of a particle moving in a magnetic field applied to transverse direction can be calculated by magnetic rigidity

$$B\rho(T \cdot m) = \frac{10\, p(GeV/c)}{2.9979} \tag{2.9}$$

Taking radius of curvature ρ = 100 mm, for 80 keV electron beam, magnetic field required to bend the beam is 125 gauss. To find out number of Ampere-turns

$$NI = \frac{Bg}{\mu_0} \tag{2.10}$$

For a pole gap of g = 18 mm, number of ampere-turns required are NI = 180. Figure 2.17 (a) present design of dipole magnet and its dimensions (b) is showing CST-EM results of 3D field distribution. Transverse magnetic field profile along z-axis are shown

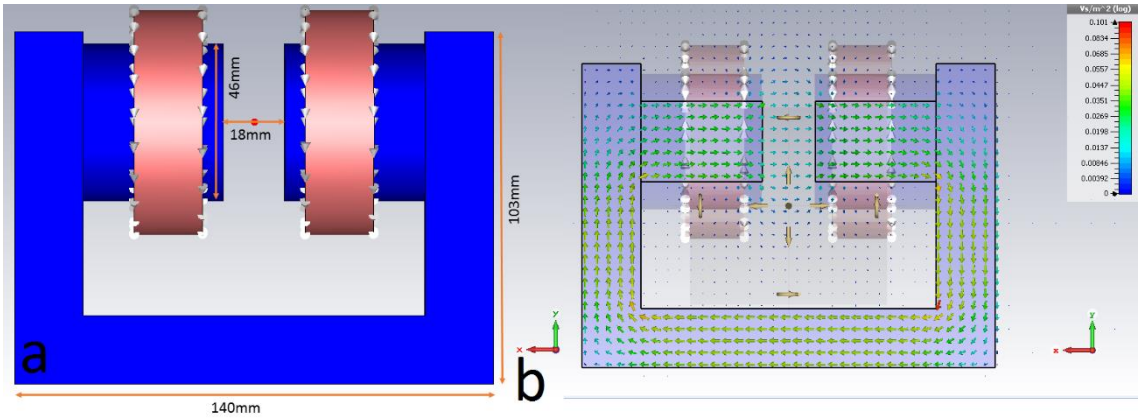

Figure 2.17: (a) Design of bending magnet and it dimensions. (b) CST-EM results of magnetic field pattern and strength.

in Fig. 2.18. Blue curve in Fig. 2.18 are measured values and red curve is showing the CST simulation results.

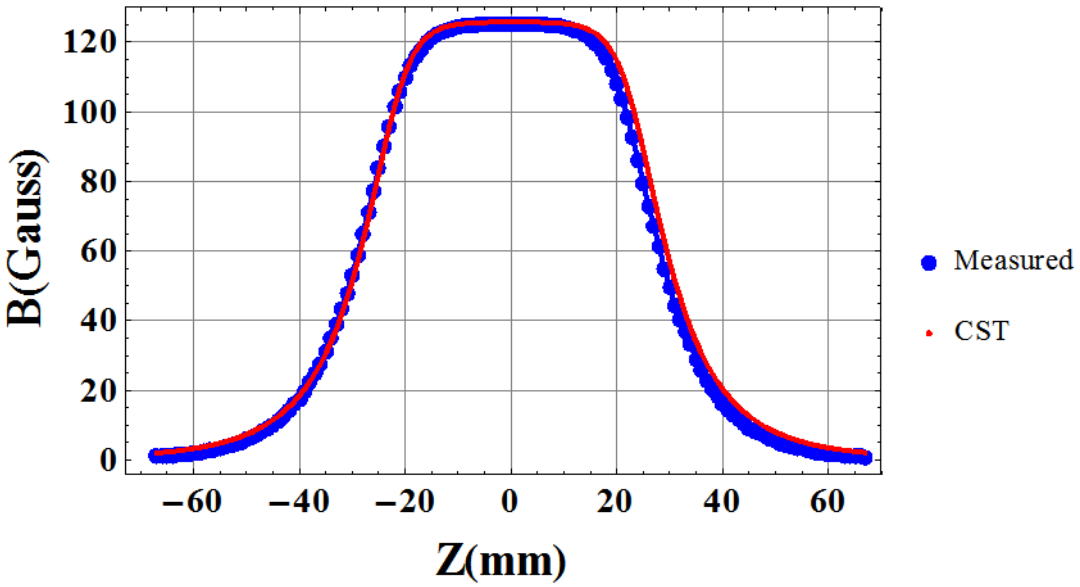

Figure 2.18: Transverse magnetic field profile along z-axis. Blue curve is measured values and red curve is CST simulation results.

Figure 2.19 is the transverse field map on y-z plane. Figure 2.20 present measured B_θ of dipole magnet as a function of current.

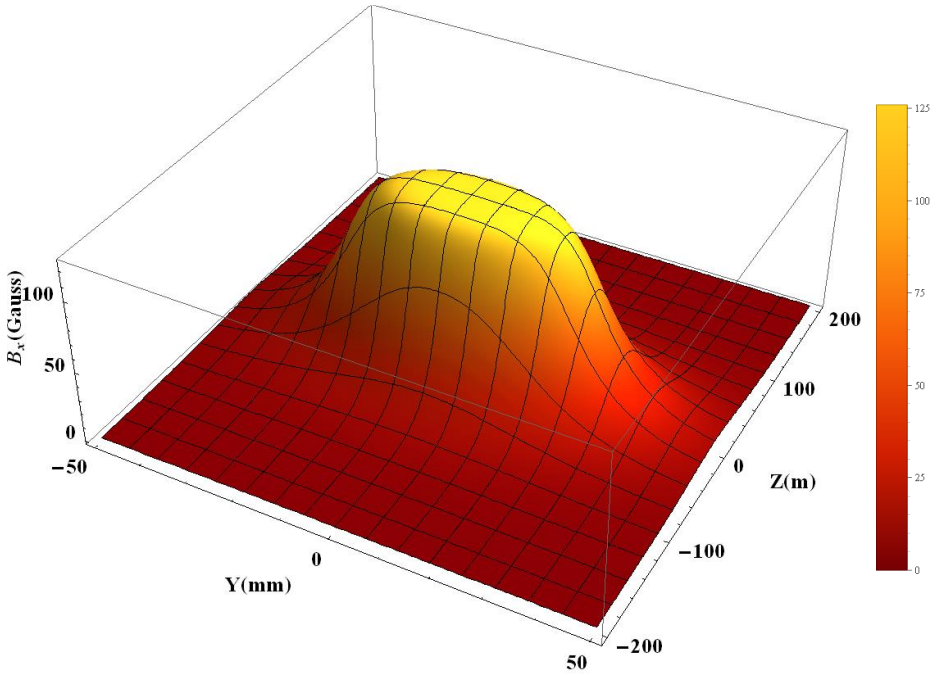

Figure 2.19: Transverse magnetic field map on Z (mm) and Y (mm) plane.

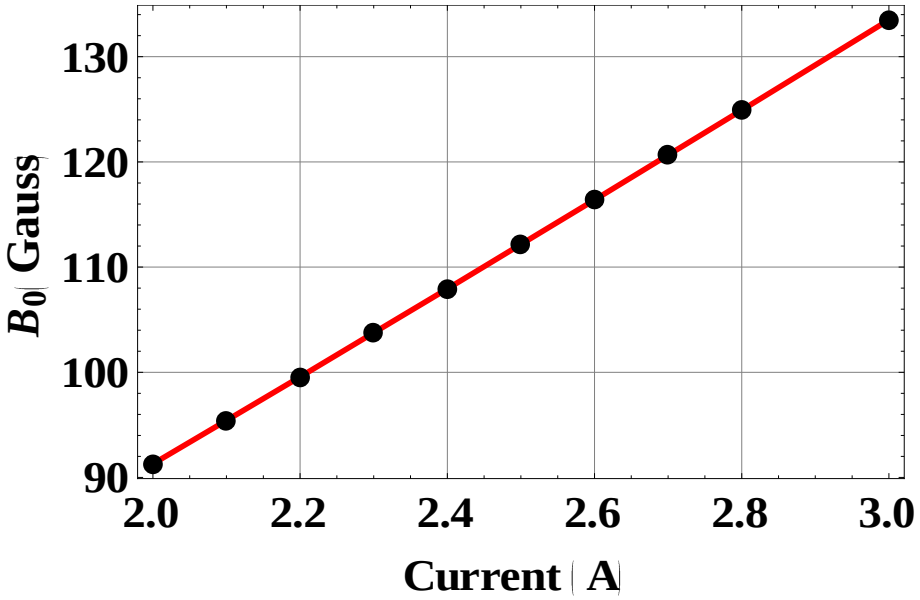

Figure 2.20: B_0 of dipole magnet as a function of current.

Magnetic field of the dipole magnet was measured by "Alpha lab Gauss meter", (Resolution 0.01 Gauss, Max. 800G) [15]. Successful injection of the electron beam highly depends upon the injection angle, which is determined by the dipole magnet strength and effective length. The effective length of dipole magnet at the current 2.79 A from measured magnetic field values is 59.4 mm and deflection angle is 43°.

$$\theta = \frac{B_0 l_{eff}}{B\rho} = 43^o \tag{2.11}$$

$$l_{eff} = \frac{\int Bdl}{B_0} = 59.4mm \tag{2.12}$$

The deflection angle and effective length from CST simulation are 61.4 mm and 44.4° respectively. The difference between measured values of the magnetic field and CST simulation arises due to imperfect coils shape of dipole magnet and parallax error in setting position of hall probe. Moreover, center of the dipole magnet was not determined precisely.

2.3.4 Differential Vacuum System

Differential pumping is a technique in which large pressure difference is maintained between different regions of a single vacuum system. The pressure difference is maintained by a small aperture between the two parts and extra pumping on the high vacuum region part.

In the straight section of beam line, a high vacuum is require to protect electron gun and transfer electron beam without any disturbance but in the storage chamber, a medium vacuum is needed to fill it with N_2 gas to observe fluorescence light due to ionization of nitrogen gas along a beam path. Differential vacuum pumping has been employed to maintain the high vacuum ($1.5 \times 10^{-6}\ mbar$) in straight beam line and medium vacuum ($1.5 \times 10^{-3}\ mbar$) in the storage magnet. A collimator of 3 mm diameter and 5 mm depth is used to separate two vacuum regions. Figure 2.21 is showing the collimator and dipole magnet. The collimator is also reducing a beam halo and related backgrounds.

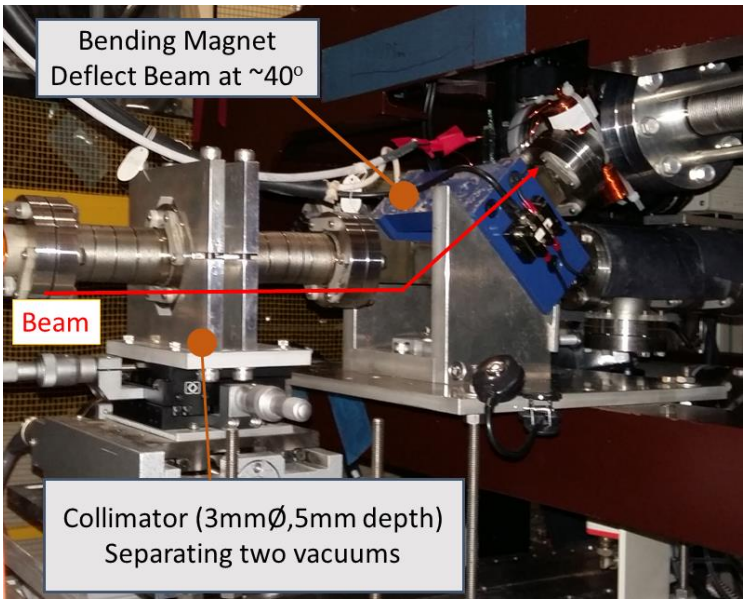

Figure 2.21: Collimator and dipole magnet.

2.3.5 Particle Tracking of Straight Beam Line in CST-PS

In order to check beam dynamics in straight beam line particle tracking in CST-PS has been carried out. For the simulation of straight beam line three components were considered namely

- Electron gun
- Magnetic lens
- Dipole magnet

There are five weak steering coils along straight beam line are present to overcome misalignment of the beam line. For CST-PS simulation, steering coils, have been ignored due to simplicity. Figure 2.22 is the representation of straight beam line, which starts from the electron gun and follows magnetic lens, collimator and bending magnet.

Figure 2.23 shows the tracking of electron beam through beam line elements. Figure 2.24-26 are transverse cross section (x-y) and phase space (x-x′), (y-y′), (x′-y′) at the exit of the electron gun, collimator and after collimator respectively. It is clear in Fig. 2.25 as electron beam reach to the collimator beam size and halo grows. The collimator removes beam halo as it is mentioned in Fig. 2.26 but it also reduced beam intensity. From electron gun, beam current was 74 μA and it reduced to 11.2 μA after the collimator. This study is not verified experimentally yet, because our major goal was to inject electron beam into the storage magnet. In near future this study will be verified experimentally.

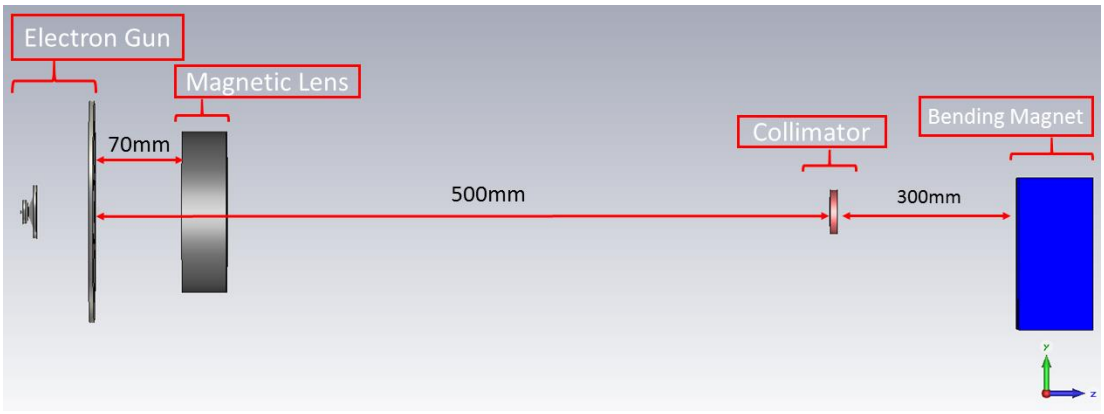

Figure 2.22: Schematic of beam line components in straight section.

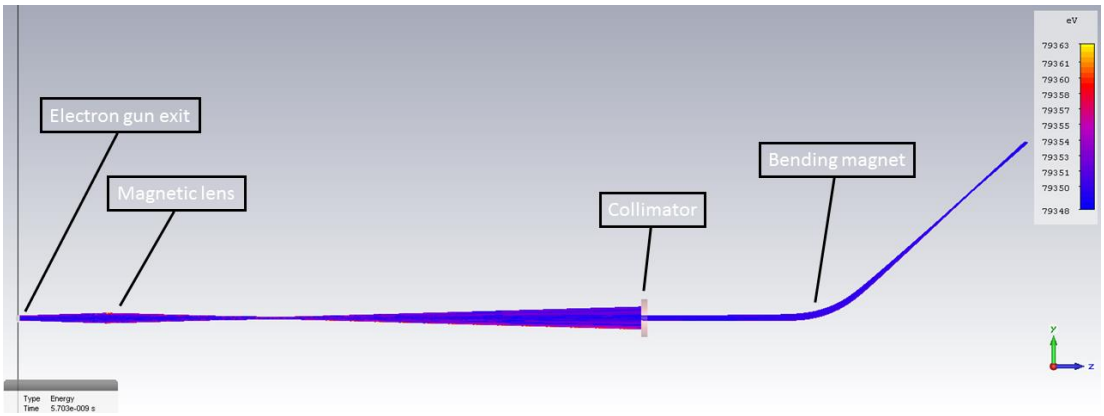

Figure 2.23: Tracking of beam through straight beam line component.

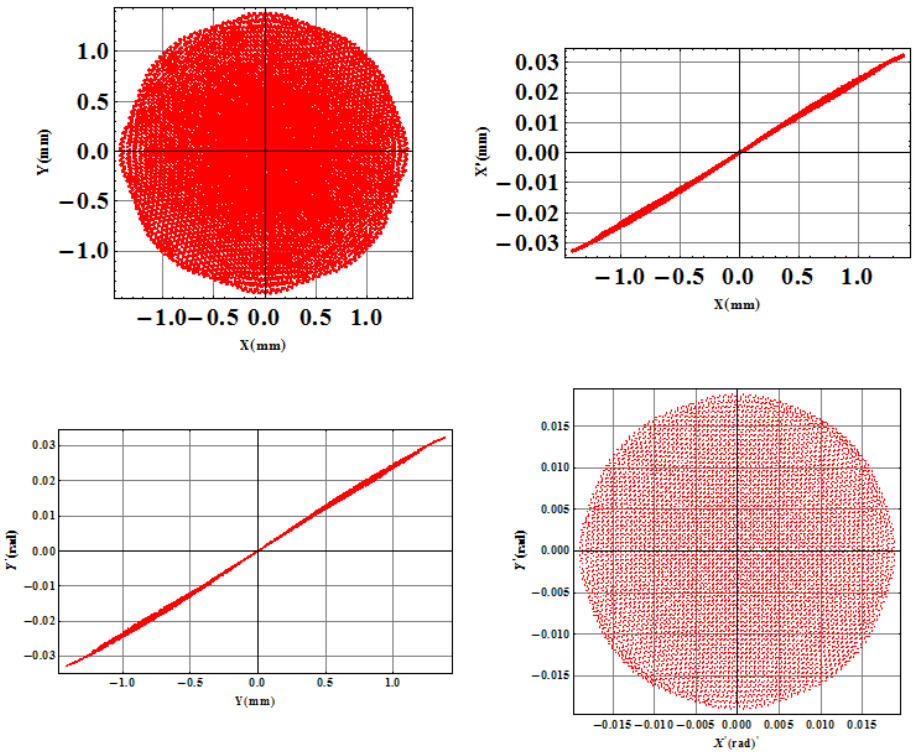

Figure 2.24: Beam phase space at the exit of electron gun

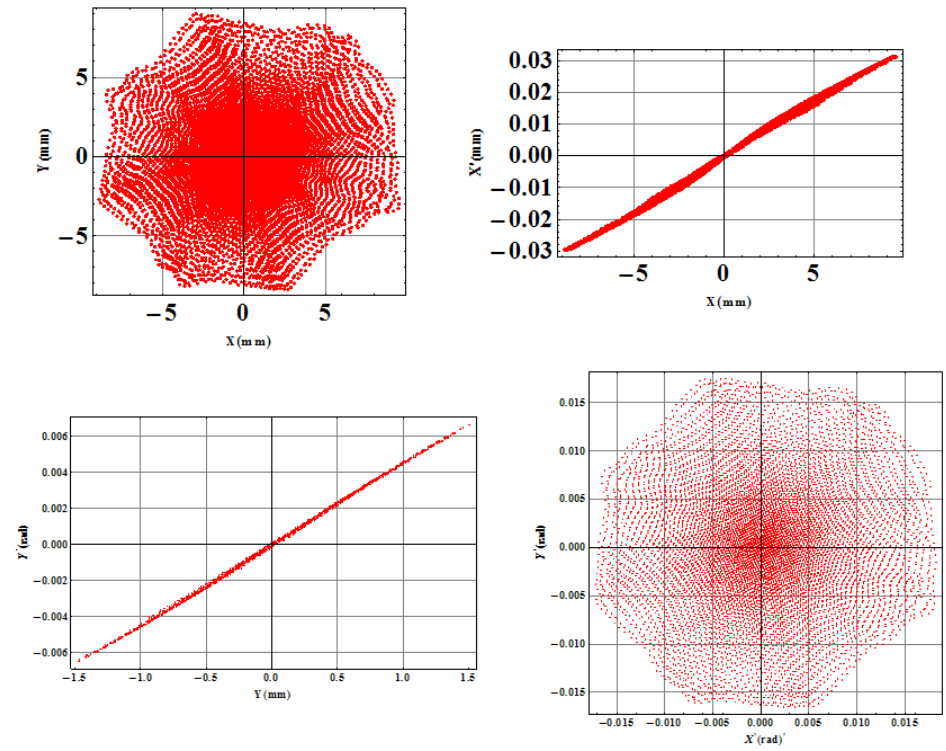

Figure 2.25: Beam phase space at the collimator

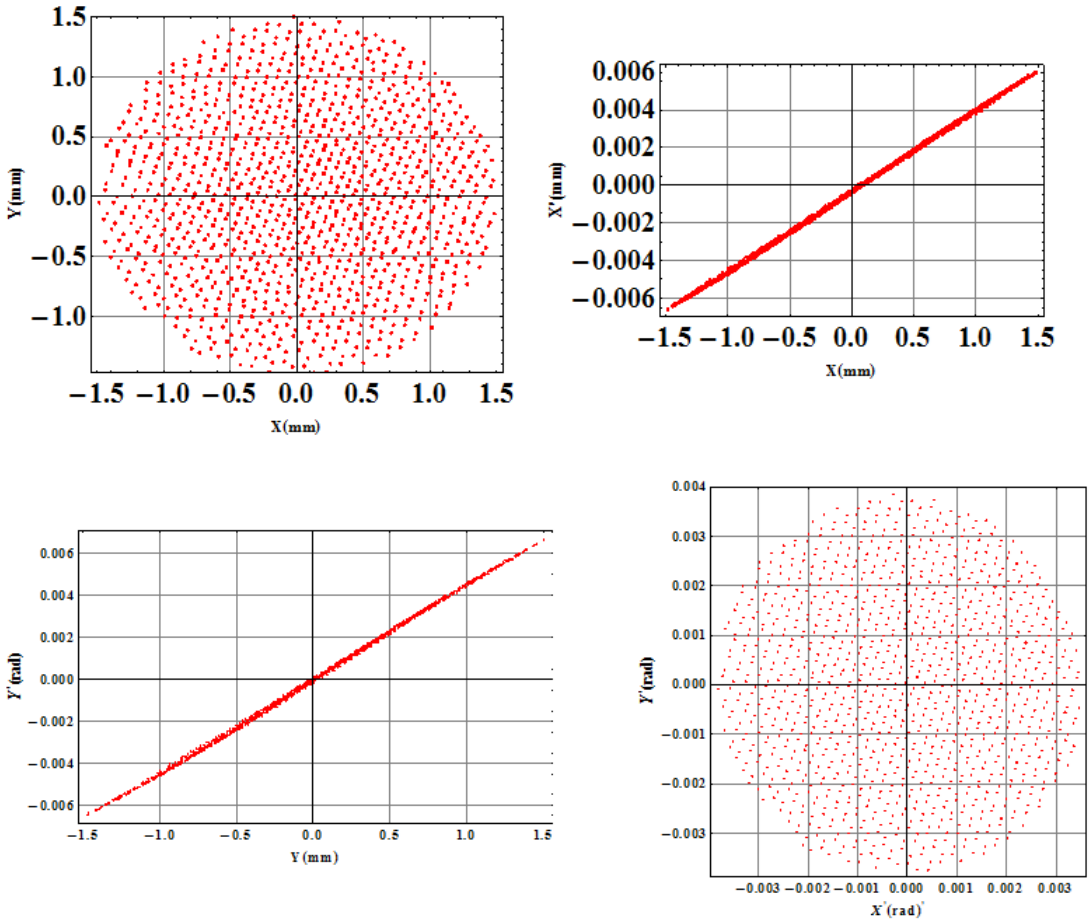

Figure 2.26: Beam phase space after collimator.

2.3.6 Storage Magnet

Storage magnet is a solenoidal electromagnet placed inside a cylindrical iron yoke of height 800 mm and diameter of 600 mm, the thickness of iron yoke is 5 mm. Top and bottom sides of the iron yoke are closed by 20 mm thick iron plate to avoid field leakage from the storage magnet. The iron poles of 120 mm height and thickness 20 mm are placed at the center of the top and bottom iron plates. Both upper and lower iron plates have four viewing windows. Upper windows are used to install CCD camera, vacuum valve and feed through for fluorescent plate. Lower windows will serve to inject electron beam and some diagnostic components.

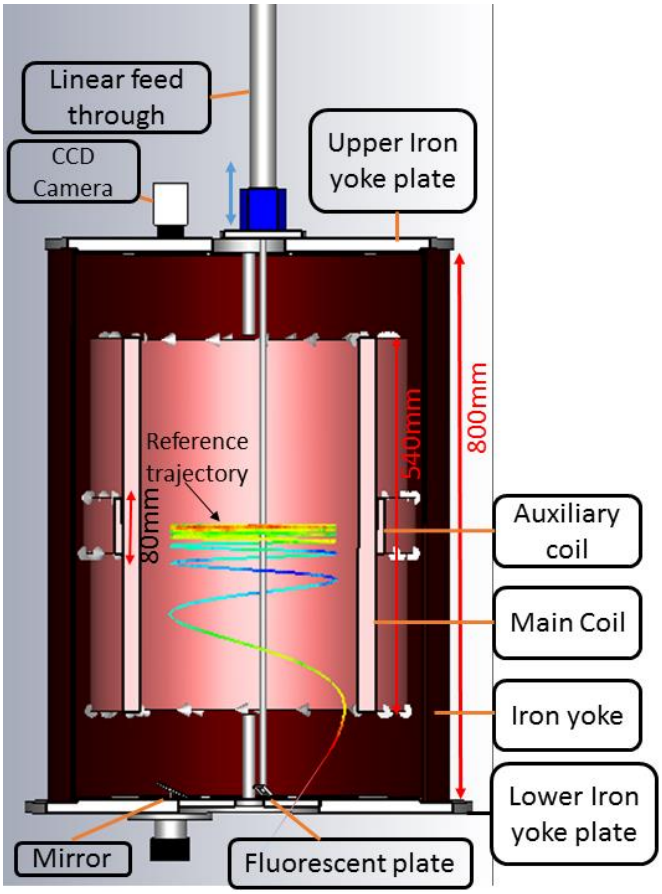

Figure 2.27: Schematic view of storage magnet with reference trajectory and monitors.

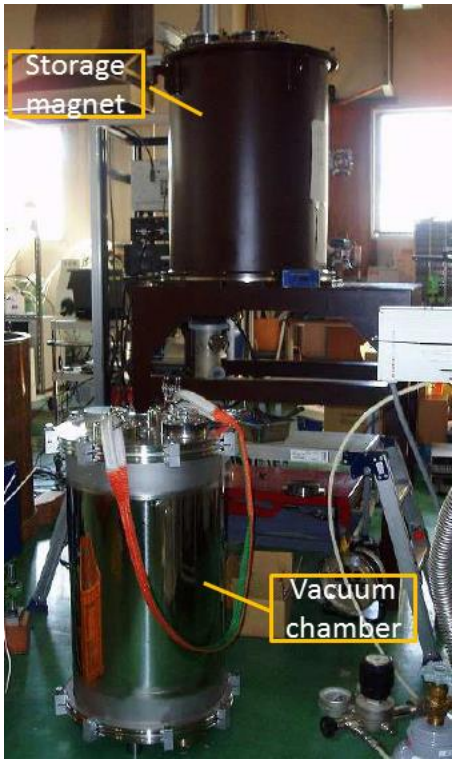

Figure 2.28: Storage magnet and vacuum chamber.

The main solenoidal coil is 540 mm in height and its inner diameter is 440 mm. The auxiliary coil of 80 mm height is mounted at the center plane of the main coil to provide weak focusing.

$$n = -\frac{R_o}{B_{oy}} \frac{\partial B_y}{\partial x}$$

Focusing condition is 0 < n < 1. Figure 2.27 is the schematic of storage magnet and also describes the beam monitoring inside storage magnet. Inside storage magnet, a vacuum chamber of height 680 mm and diameter of 400 mm is installed, that is shown in Fig. 2.28.

2.3.6.1 Field Measurement

The magnetic field is measured using a Gauss meter (Lakeshore model 460) with a three-axis hall probe. The hall probe was movable vertically and radially. Figures 2.29 show results of field measurements as a function of vertical position (z). The main drive current was fixed at 8 A. Colored data correspond to different drive currents (0 ~ 10A)

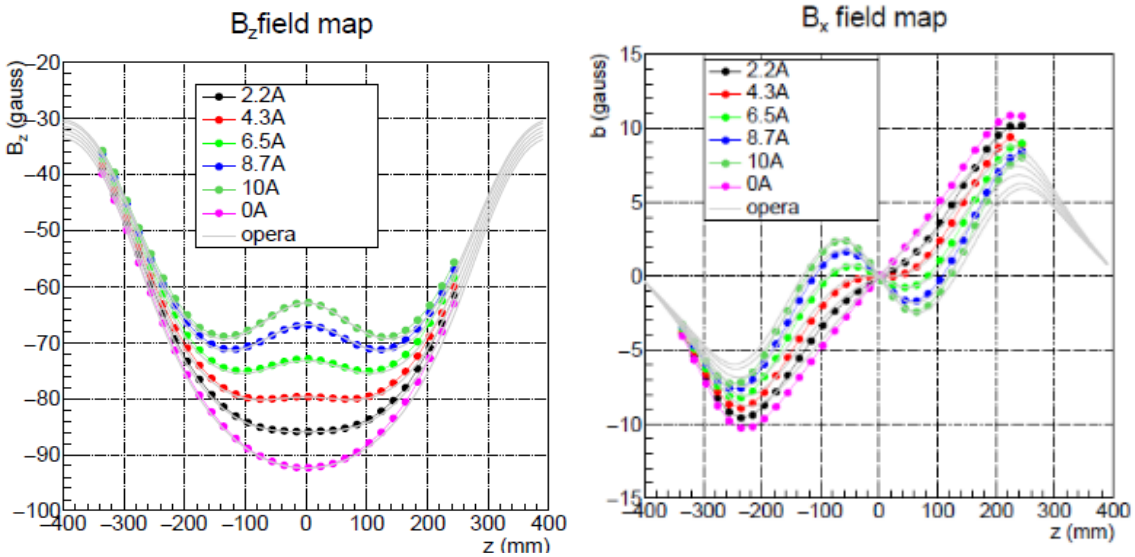

Figure 2.29: Left. Measurement of B_Z component as a function of vertical position. Color data correspond to different auxiliary coil current Grey data represent OPERA results. Right: B_X component as a function of vertical position.

of the auxiliary coil. The uncertainty of these measurements is estimated to be smaller than 1 gauss. Gray solid lines show OPERA [16] calculations for comparison.

There is discrepancy between radial component in measured values and OPERA simulation as shown in Fig. 2.29 right. During field measurement, some flanges were open but this effect is not included in OPERA model.

2.3.6.2 Particle Tracking in Storage Magnet

Particle tracking is one of key calculation to determine particles motion inside storage magnet. Tracking calculations has been carried out in CST-PS studio. The magnetic field of storage magnet is calculated at main coil current 8 A and auxiliary coil current 4 A which is correspond to central field strength B_0 = 83 gauss and field index value n=0 at median plane of storage magnet.

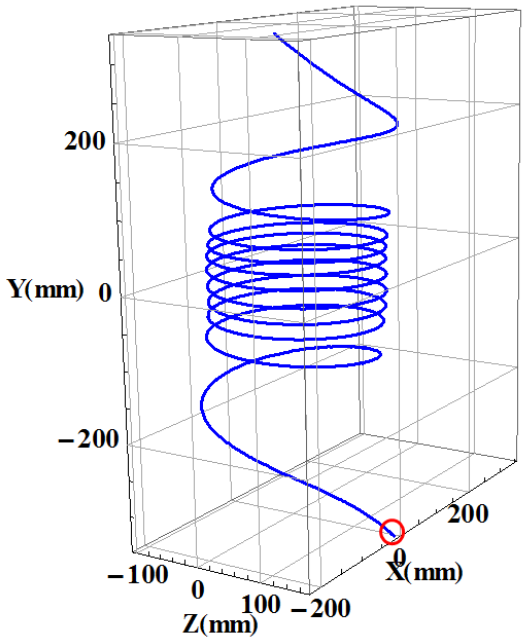

Figure 2.30: Single particle tracking in storage magnet field. Red circle is showing the starting point of tracking calculation.

Figure 2.30 is showing the single particle tracking in the storage magnet field, red circle

is the entering point of particle. Beam encompass diameter of ~24 cm in the median plane of the storage magnet.

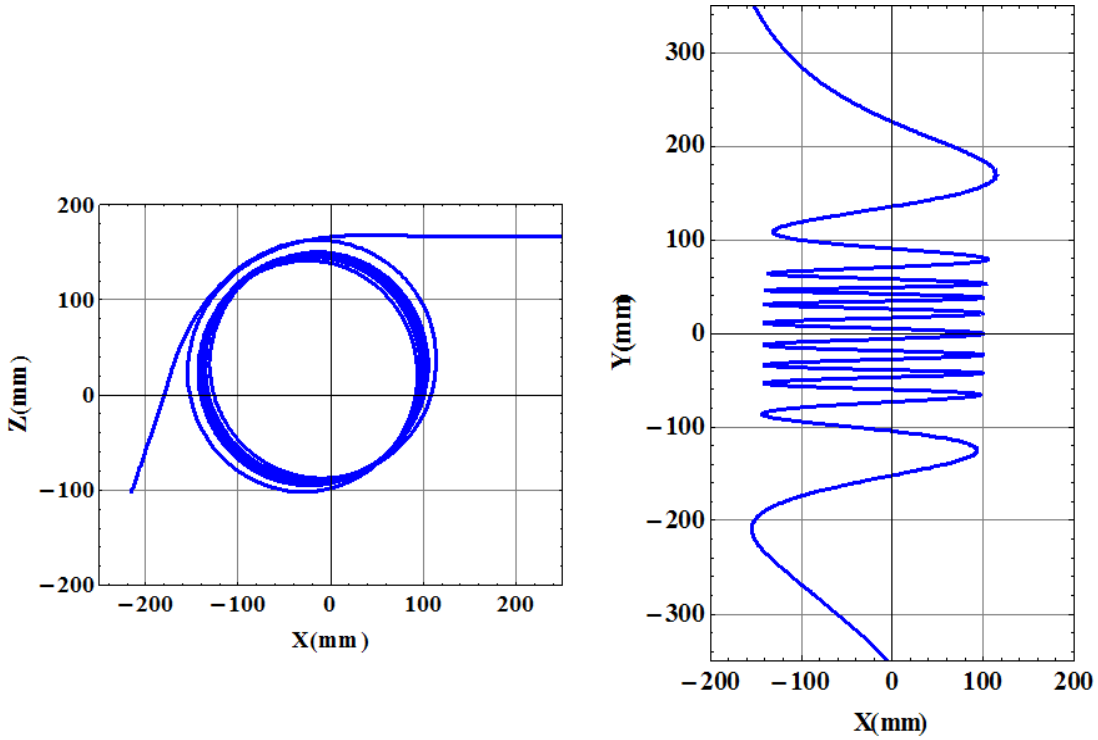

Figure 2.31: Left: Single particle tracking in the x-z plane of the storage magnet, which encompass ~24 cm diameter orbit. Right: Single particle tracking in x-y plane of the storage magnet.

Figure 2.31 left is the representation of single particle trajectory in the x-z plane which shows the diameter of tracking ~24 cm. Figure 2.31 right is showing the x-y plane of trajectory as it moves in the upward direction vertically.

2.4 Second Stage Upgrade of Straight Beam Line

The second stage of SITE aims to upgrade following three items

- DC beam to pulse beam
- Magnetic Kicker to guide electron pulses to very center of storage chamber
- Beam monitors to measure storage time of electron beam and kicker efficiency

Development of electric chopper system for the generation of pulse beam has been completed and will be described in the next section in detail. Magnetic kicker and beam

monitors are still under plan stage.

2.5 Electric Chopper System

To produce pulse beam for the SITE, the original plan was to use RF cavity but due to high cost of RF source, it was decided to utilize some cheap and efficient option. Fast response, simple structure and low cost make electric chopper system best choice for the generation of pulse beam.

For the electric chopper system structure designing process following aspects were

- A maximum effective field in the same deflecting voltage condition
- A minimum loaded capacitance of electrodes to achieve the fast rise/ fall time

The chopper voltage depends on the electron beam energy, the distance, and length of the plates and on the beam stop location. The required deflection voltage can be calculated by the following equation

$$V_d = \frac{\theta(\gamma mc^2)\beta^2}{l} d \tag{2.13}$$

Where V_d is the deflecting voltage, l is the length of plate, θ is required deflection angle, d is the gap length. $\gamma \ and \ \beta$ are relativistic factor of beam.

$$y = \frac{V_d l}{2dV_{acc}} (D`) \tag{2.14}$$

Equation 2.14 present the dependence of y on different parameters. Where y is distance on which beam deflect, V_{acc} is the accelerating voltages of beam, l is the length of plate; V_d is the deflecting voltage, d is the gap length. $D`$ is the distance from the middle of plates to dump location.

In our case, the electrode length was chosen 35 mm and mutual separation between electrodes plates are 10 mm. The collimator to control beam halo and for differential vacuum system will serve as a beam dumper for chopper system. The electron beam of 80 keV will be deflected on the collimator at a distance of 20 mm, which corresponds to the deflection angle of 0.04 rad, which require deviating voltage of 1.6 kV. Schematic layout of chopper system is given in Fig. 2.32. Table 2.4 presents geometrical parameter of chopper system.

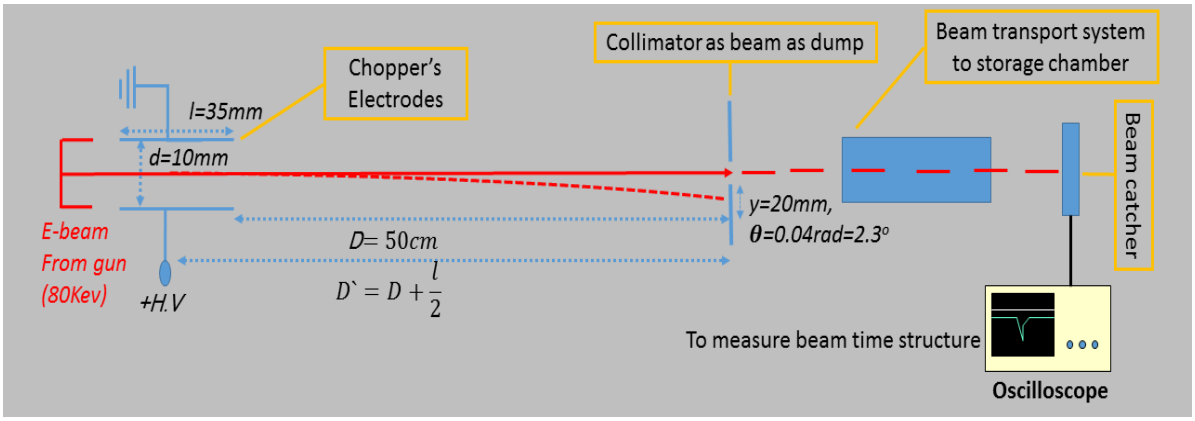

Figure 2.32: Schematic layout of chopper system.

Table 2.4: Geometrical parameter of electric chopper.

Parameters	Values
Injected beam energy	80 keV
Chopper Deflecting voltages	1.6 kV
Electrode length	35mm
Aperture (width×height)	20mm×10mm
Deflection angle	0.04rad

Figure 2.33 is showing the effect of electrode length on required deflecting voltages and electric field to deflect electron beam on collimator. As mentioned in the equation 2.13 the required deflecting voltages to deflect the beam of constant energy and angle reduce as we increase the length of chopper electrodes.

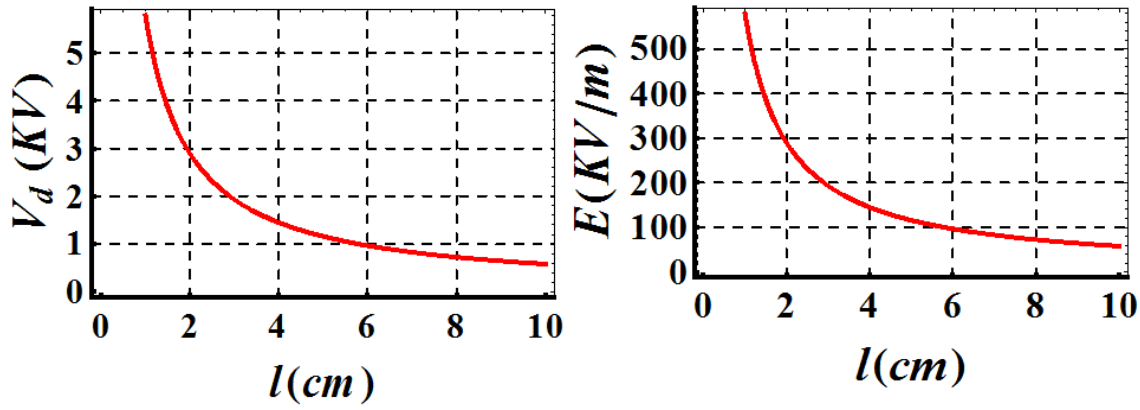

Figure 2.33: Left: Effect of length of chopper's electrode plates on required deflecting voltages. Right: Effect of electrodes length on electric field.

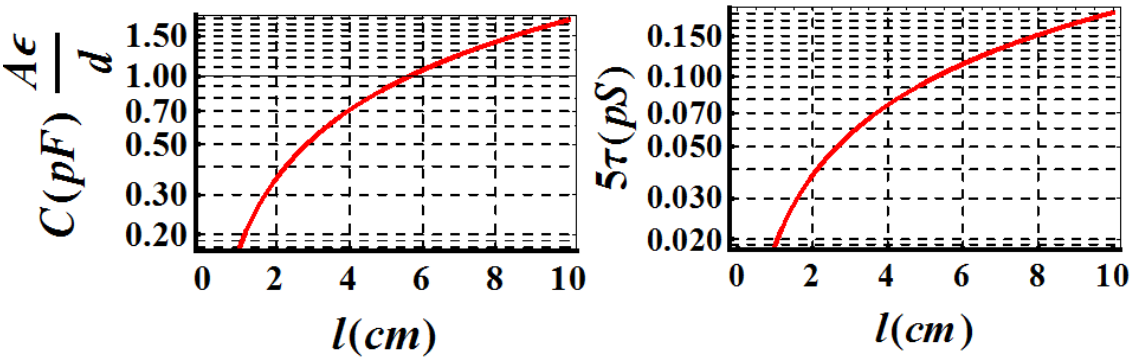

Figure 2.34: Left: Capacitance of chopper plates as a function of chopper electrode length. Right: Charging time of chopper electrodes as function of electrode's length.

Capacitance and full charging time of chopper plates also depend upon length of chopper's electrodes. Figure 2.34 present the effect of electrodes length on capacitance and charging time.

2.5.1 Electrical Design

The schematic of electrical design of the chopper system is presented in Fig. 2.35. The high voltage power supply is connected to pulse generator, which acts like a switch. Pulse generator alternatively connects the electrode to ground and to the positive and negative high voltage power supply following the timing signal repetition rate and pulse width from a function generator (trigger).

The key component of chopper system is PVX 4140 pulse generator. Agilent 81101A function generator is used to feed timing signal for pulse generator. Parameters for chopper's power supply system are given in Table 2.5.

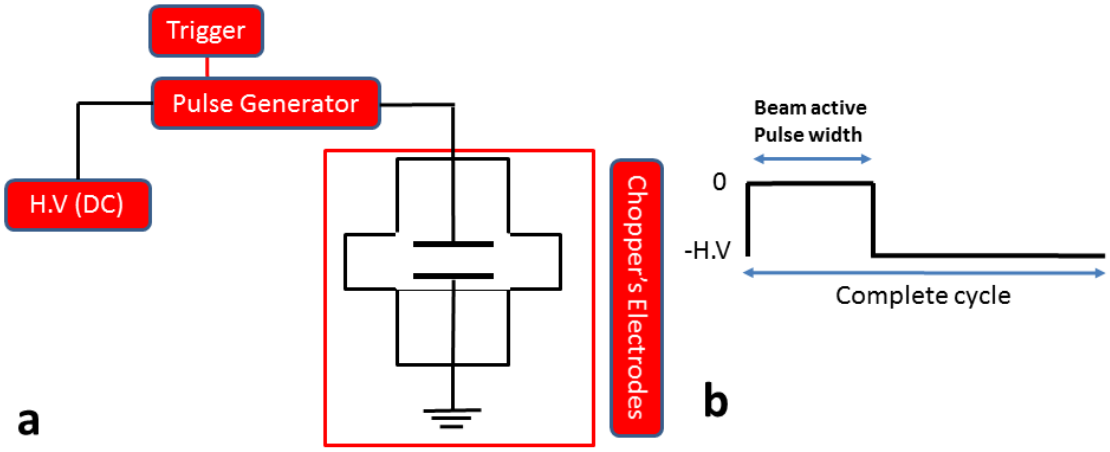

Figure 2.35: (a) Electrical design of chopper system. (b) Ideal beam pulse generated by electric chopper system.

Table 2.5: Electrical parameters for chopper system.

Parameters	Values
Max Voltage PVX 4140	±3.5 kV
Pulse rise/ fall time	≤25 ns 3500V (load)
Loaded capacitance	50 pF
Pulse width	50 ns to DC Controlled by input gate Agilent 81101A
Pulse Recurrence Frequency	Controlled by input gate 50Hz, Agilent 81101A

2.5.2 Mechanical Design

The mechanical assembly of chopper system is shown in Fig. 2.36. A cross beam pipe of asymmetric diameter is used to host the electrodes. Bigger diameter pipe is used to produce easy support structure for the insertion of electrodes. Each electrode is consist of a plate of 3 mm thick stainless steel sheet supported by two a ceramic column. They are inserted from opposite sides and their vacuum flange supports each one. The ground electrode is directly connected to the flange while the polarized plate is welded to the Miniature High Voltage (MHV) feed-through connector. Figure 2.37 (Left) present the support structure and feed through connection to the H.V plate, Right is showing the cross section of electrodes assembly in the vacuum chamber. The ceramic feed through is a standard 5 kV single ended coaxial MHV connector.

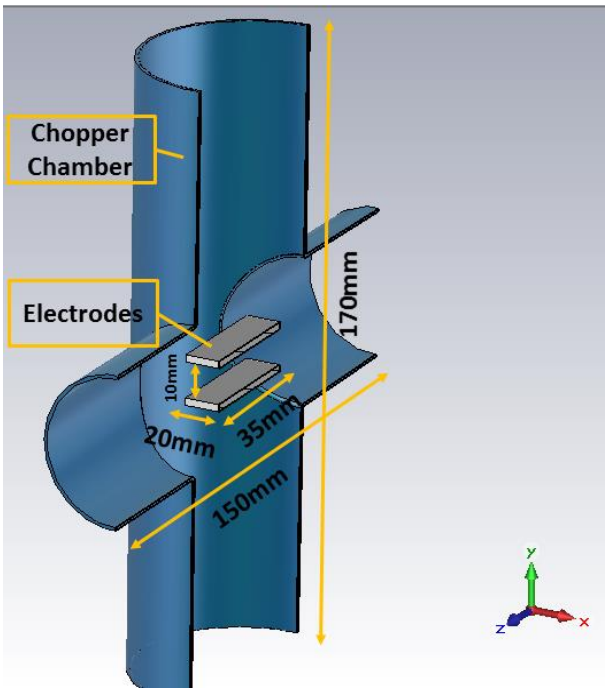

Figure 2.36: Mechanical structure and dimension of chopper system.

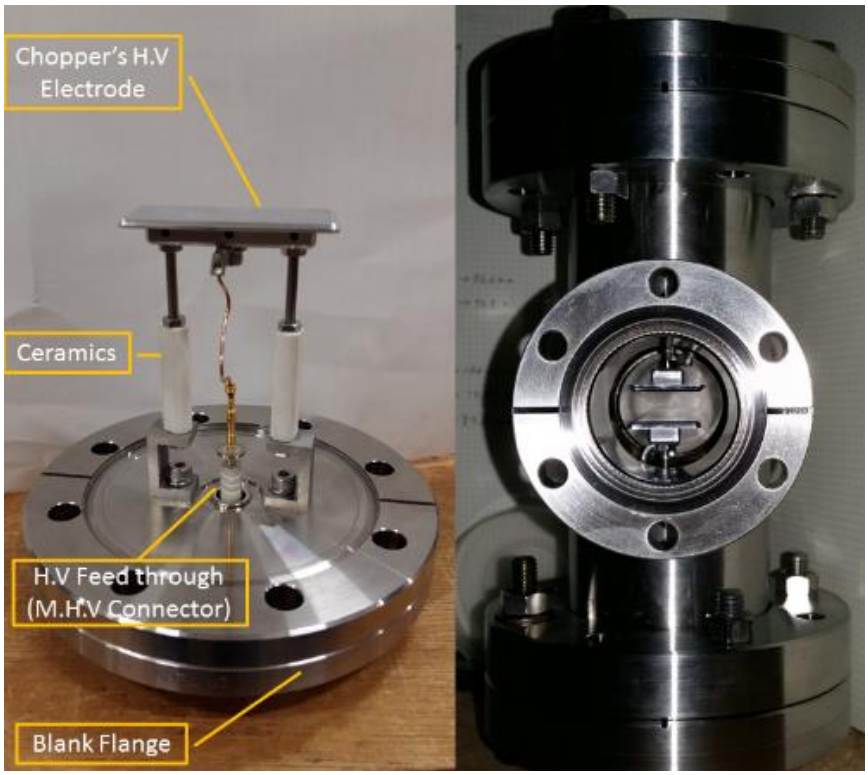

Figure 2.37: Left: H.V electrode and its support. Right: Chopper's electrodes in vacuum chamber

2.5.3 CST Simulation

To check electric field profile and examined the effect of maximum electric field on vacuum chamber walls, simulation of chopper system is carried out in CST-EM studio. 1.6 kV were applied to the lower electrode plate while upper plate and vacuum chamber were at ground potential. Figure 2.38 left shows the potential contours over cross section of chopper system and right present the electric field profile over cross section of beam pipe. The equipotential lines near high voltage electrode are dense which indicates a large electric field in the z direction. Maximum field calculated from analytical formula and from simulation are in agreement with each other. Figure 2.39 present the uniform region of electric field in the x-z plane of chopper's plates.

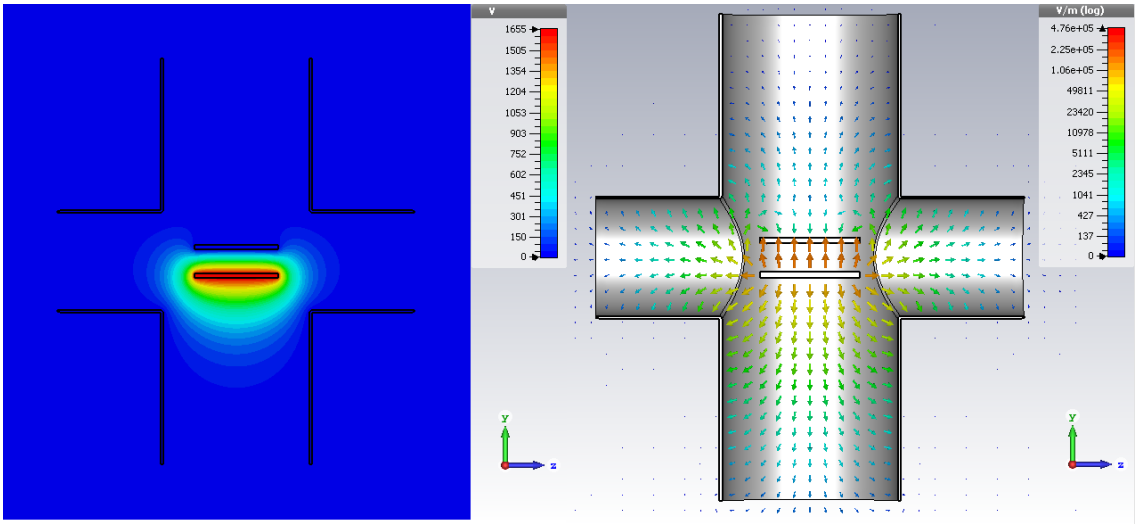

Figure 2.38: Left: Potential contours on the electrodes. Right: Electric field pattern of electrodes in vacuum chamber of chopper system.

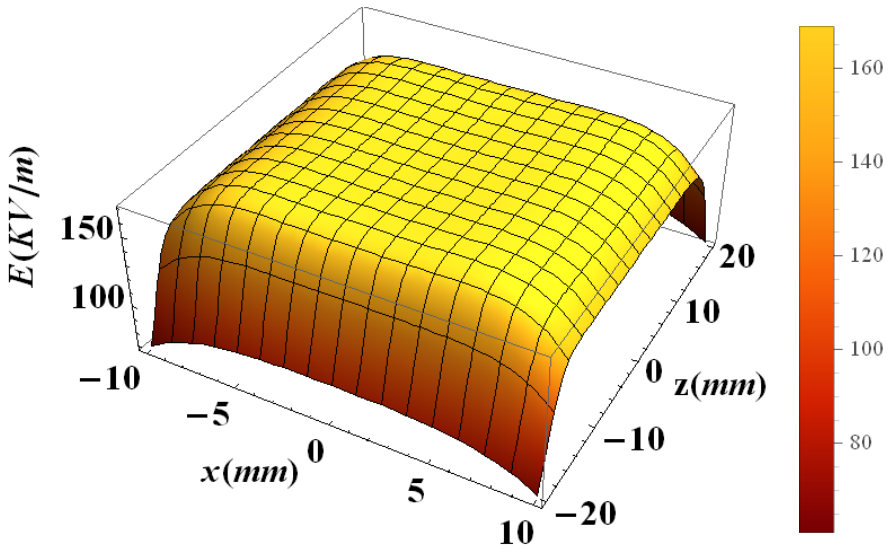

Figure 2.39: Electric field profile in (x-z)-plane.

2.5.4 Experimental Setup

All electrical components used in chopper system are commercially available devices.

The electrical components used are as follow

1) Pulse generator: DXI PVX 4140

2) Function generator: Agilent 81101A

3) Matsuda H.V power supply

4) Oscilloscope: Tektronix

The PVX-4140 pulsar is used to generate pulse voltage for chopper system. The PVX-4140 features single-ended output pulses from ground to +3500V or from ground to -3500V, and can also generate pulses originating from a voltage offset from ground. Rise and fall times is 25 ns and minimum pulse width is 50 ns with maximum frequency of 30 kHz. H.V power supply from MATSUDA Precision [17] is used to provide H.V to the pulse generator. Agilent 81101A function generator [18] is used to trigger the PVX-4140 pulse generator [19]. It offer maximum frequency 50 Hz and an individually adjustable pulsed width and pulse delay. 5 V output from function generator is used to trigger pulse generator. Detail setup and equipment are depicted in Fig. 2.40. Figure 2.41 shows the output of 100 V from pulse generator.

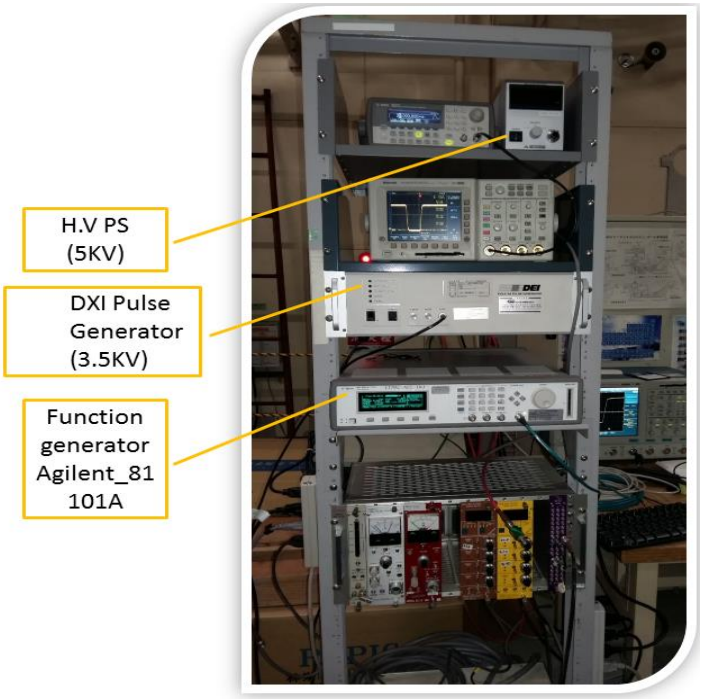

Figure 2.40: Electrical component setup for chopper system (DC power supply, pulse generator, function generator)

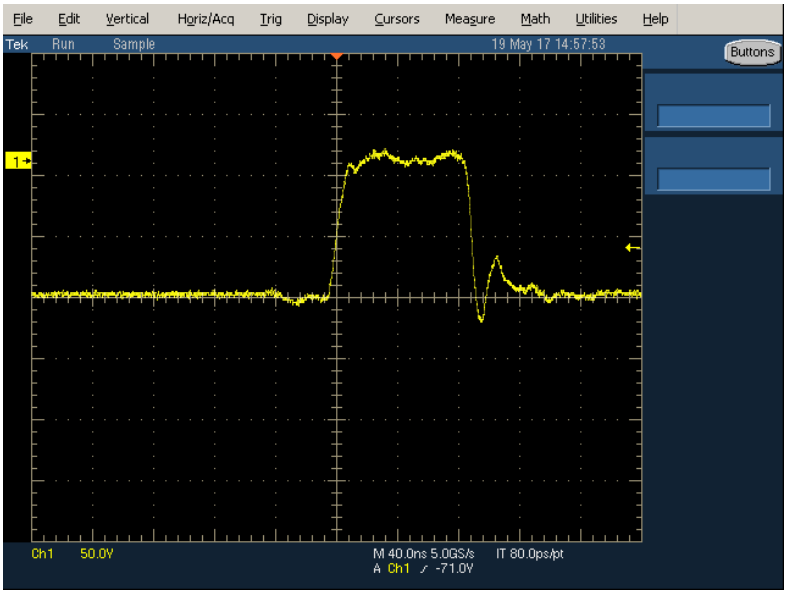

Figure 2.41: Output from PVX 4140 Pulse generator on Tektronix 5054 Oscilloscope

Chapter 3

Beam Commissioning and Results

Conventional fluorescent screen monitors were used to detect electron beam transverse profile during the commissioning and operation of SITE in the straight beam line. In order to monitor the electron beam in a non-interceptive way, storage magnet was filled with nitrogen gas and fluorescent light due to the excitation of nitrogen gas was observed using a Charge Coupled Device (CCD)-camera. In this chapter setup of beam monitors in straight beam line and storage magnet and their results will be described in detail. Several challenges had to overcome during the beam commissioning from the straight beam line to the storage magnet. Those problems will also be discussed in this chapter.

3.1 Beam Commissioning and Monitors in Straight Beam Line

Fluorescent screen (FS) monitors is a simple interceptive beam diagnostics device to measure the transverse beam profile. When a charged particle collides with a material its energy loss can be converted to fluorescence light. The released light output from FS is in the optical wavelength range (450 nm < λ < 700 nm). A CCD-camera can be used to capture light from FS. High dynamic range, no absorption of emitted light, radiation hardness, fast decay time and good mechanical properties makes FS one of best choice for intercepting beam diagnostic [21-22].

The FS material is made of Al_2O_3 and doped with Cr activator. Black and White (B/W) Hamamatsu Chilled CCD camera (model C5985) and digital camera were used to capture fluorescence light. FS monitors were installed at the three different locations on the straight beam line to investigate beam profile at those locations. First diagnostic FS is placed on the collimator perpendicular to the beam direction and the light extraction

mirror was placed at 45^{o} with respect to the FS. Mirror guide fluorescent light to the digital camera. Figure 3.1(a) is the schematic of first FS monitor and (b) is showing the mirror and FS monitor used in experimental setup.

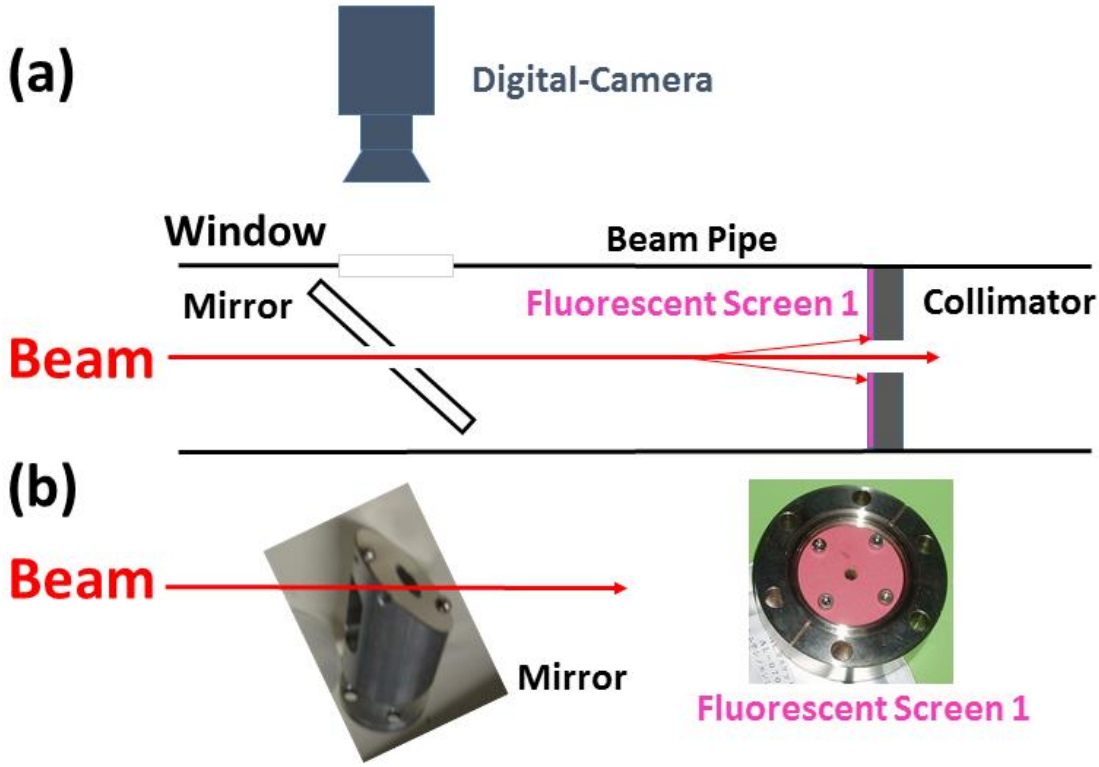

Figure 3.1: (a) Schematic of the first FS monitor (top view). (b) Mirror and FS used in first monitor.

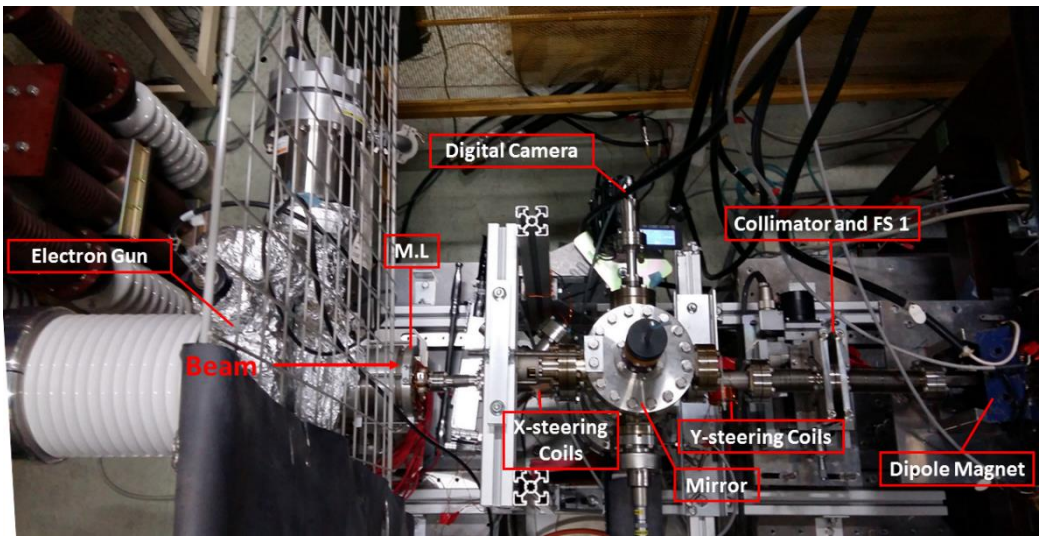

Figure 3.2: Top view of straight beam line and first FS monitor.

Figure 3.3: Beam profile from first FS monitor.

Beam profile from the first FS monitor is shown in Figure 3.3. Second diagnostic FS monitor is placed at the end of straight beam line at 45^{o} with respect to the beam direction and CCD camera-1 is adjusted below the screen to capture fluorescent light. The detail setup is depicted in Fig. 3.4. Figure 3.5 (a) shows the schematic of second FS monitors.

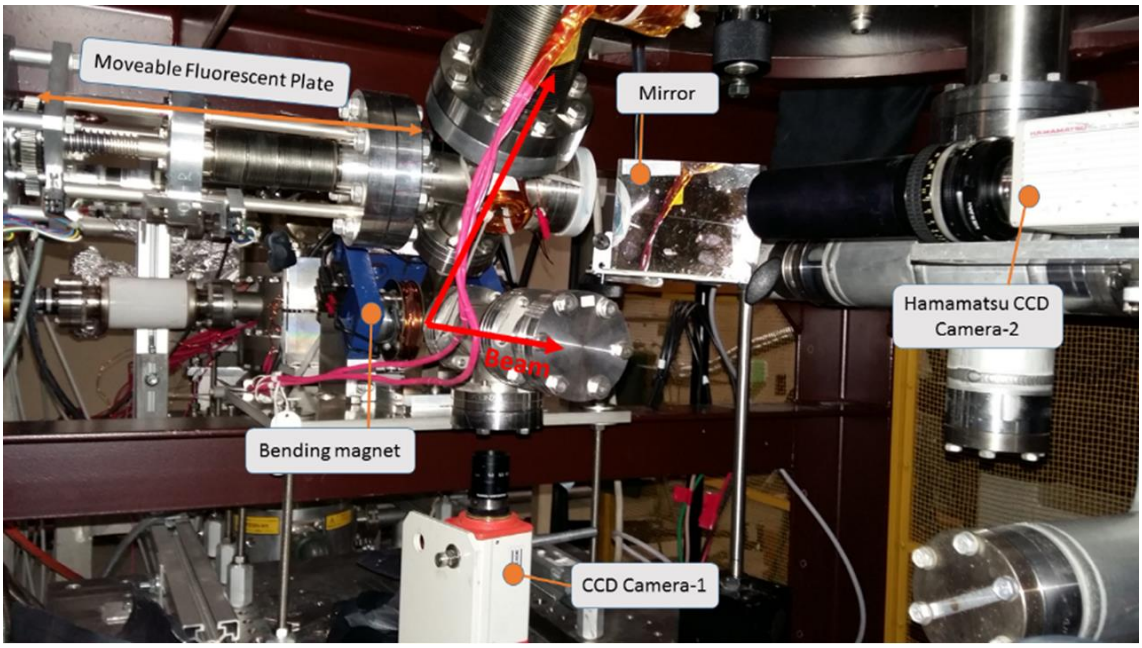

Figure 3.4: Beam diagnostic at injection region.

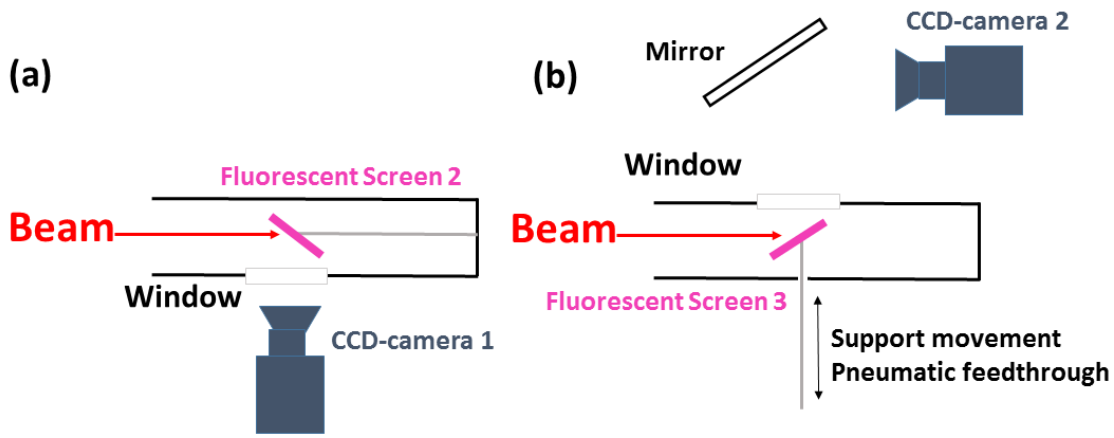

Figure 3.5: (a) Schematic of interceptive FS monitor used in straight beam line (b) and on the injection pipe.

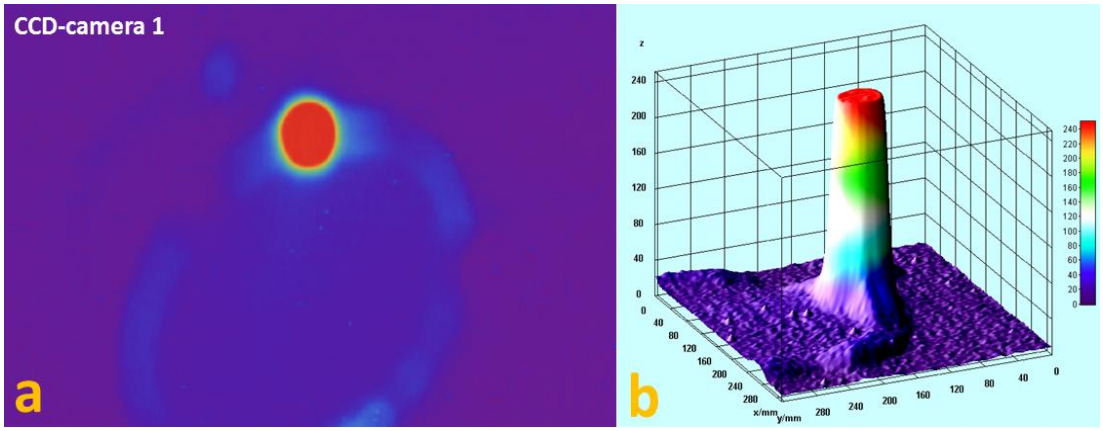

Figure 3.6: (a) Beam spot on FS monitor in straight section of beam line. Original black and white image was converted to false color for better visibility. (b) Intensity of beam as a pixel values on x and y axis.

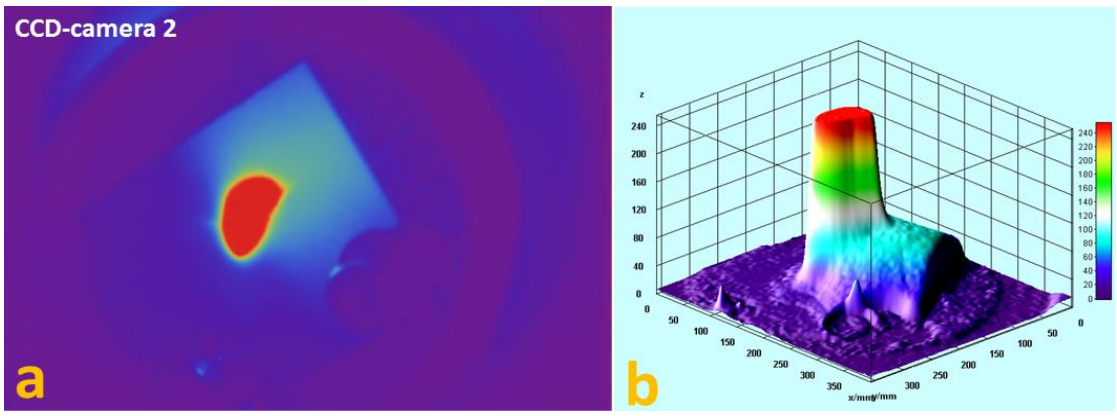

Figure 3.7: (a) Beam spot on FS monitor after dipole magnet. Original black and white image was converted to false color for better visibility. (b) Intensity of beam as a pixel values on x and y axis.

Third FS monitor is placed after bending magnet and attached to pneumatic feed through. Pneumatic feed through inserts the FS into the injection pipe and vice versa. The emitted fluorescent light from the FS was guided through a mirrors and glass viewport to the CCD camera 2. This setup is elaborated in Fig. 3.4 and 3.5 (b), CCD-camera-2 was used to capture fluorescent light from third FS.

In order to make pictures more visible image processing of black and white CCD camera figures had been done in MATHEMATICA [23] and "imagej" [24] software. False colors have been added to the original B/W photos for better visibility.

Figure. 3.6 (a) is the beam profile from second FS monitor and captured by CCD-camera 1, (b) represent the x-y projection of beam in terms of image pixel. Figure 3.7 (a) is the beam profile from the third FS monitor, which is placed after the bending magnet and image was captured by CCD-camera 2. Figure 3.7 (b) represent the x-y projection of beam in terms of the image pixels. Beam profile after dipole magnet is twisted vertically due to focusing effect of bending magnet. When we filled storage magnet with N_2 gas it also results in increased pressure in injection region. Due to the excitation of nitrogen gas in the injection region path of the electron trajectory become visible. Detail of this phenomena will be described in section later section. Figure 3.8 is depicting the electron beam path when it enters into the storage magnet. Red dotted line is the encasing of beam trajectory which presented as Region of Interest (ROI).

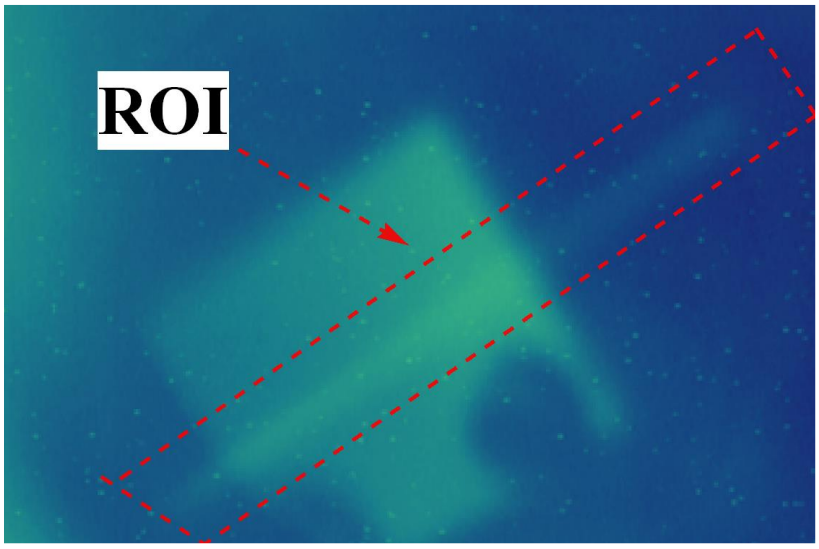

Figure 3.8: Beam trajectory in injection region while Storage chamber was filled with N_2 gas.

3.2 Issues during the Beam Commissioning

Many issues have to overcome during the beam commissioning from the straight beam line to the storage magnet. Some modifications in the original plan were made in order to overcome these problems. Before discussing the detail of results from the storage magnet, challenges faced during the beam commissioning into the storage magnet will be described briefly. Following are some selective issues, those will be described briefly

- Beam hit at injection pipe
- Field leakage from injection hole
- Alignment stage for storage magnet
- Wrong polarity of auxiliary coil of storage magnet

3.2.1 Beam Hit at the Injection Pipe

In trial operation of beam commissioning in the storage magnet we did not succeed in injecting beam into the storage magnet due to the particular shape of the beam pipe. Old beam had bellows on both sides of pipe which makes it bend in the center region as shown

in Fig. 3.9. Red circle in Fig. 3.9 is showing the hit point with temperature 43.3°C. Due to this center bend at injection pipe, beam couldn't enter into the magnet. Using thermal camera beam hit at injection pipe has been confirmed as it is shown in Fig. 3.10.

To overcome this problem a new beam pipe was prepared with straight pipe near the injection and installed on the beam line as shown in Fig. 3.11. After the replacement of beam pipe, electron beam successfully injected into the storage magnet and confirmed by using FS monitors.

Figure 3.9: Old and new injection pipe for the injection of electron beam in storage magnet.

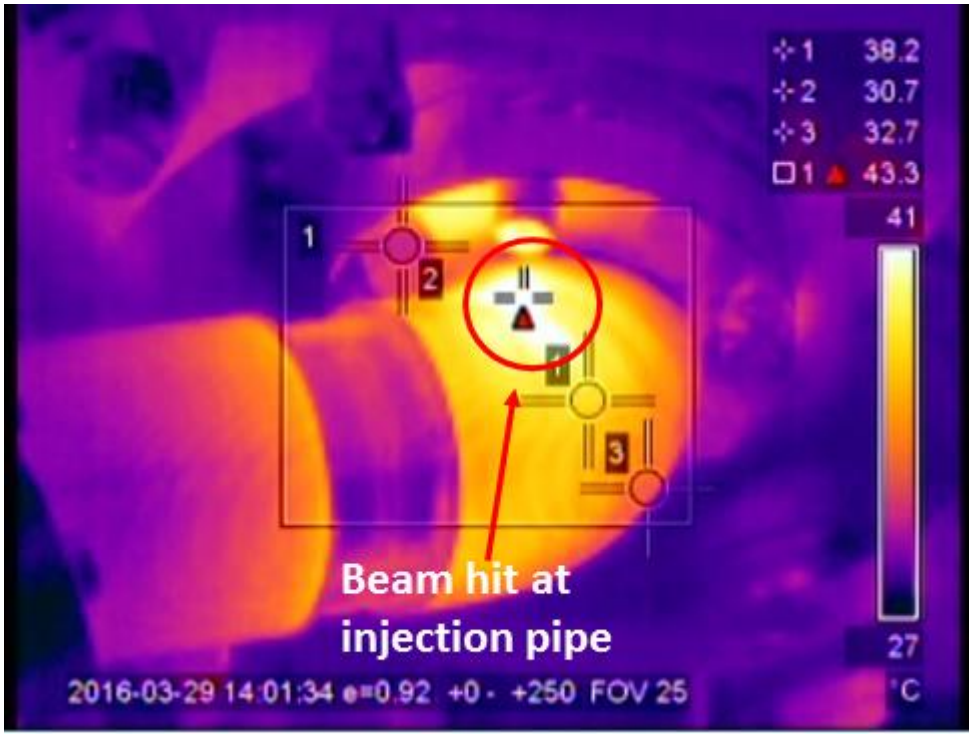

Figure 3.10: Beam hit at the injection pipe. Red circle is showing the hit point with temperature 43.3°C.

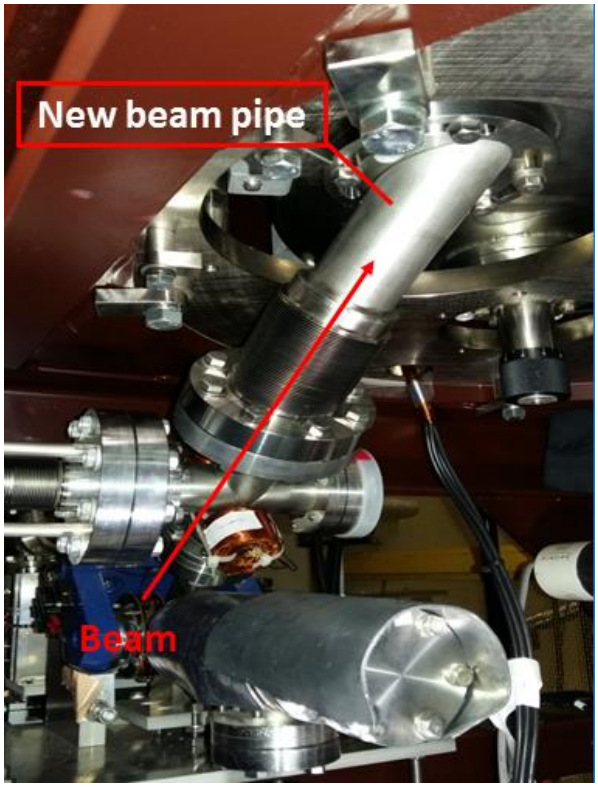

Figure 3.11: New injection beam pipe.

3.2.2 Field Leakage from the Storage Magnet

Successful injection highly depends upon on the incidence angle of the electron beam into the storage magnet. In trail operation of beam injection, it was found that injection angle cannot be controlled by only one bending magnet due to the leakage field from injection hole of storage magnet as depicted in Fig. 3.12. Second dipole magnet was installed on injection pipe to compensate the effect of the leakage field from the storage magnet as shown. Figure 3.13 is showing the second dipole magnet. Figure 3.14 represents the second dipole magnet on the injection beam pipe.

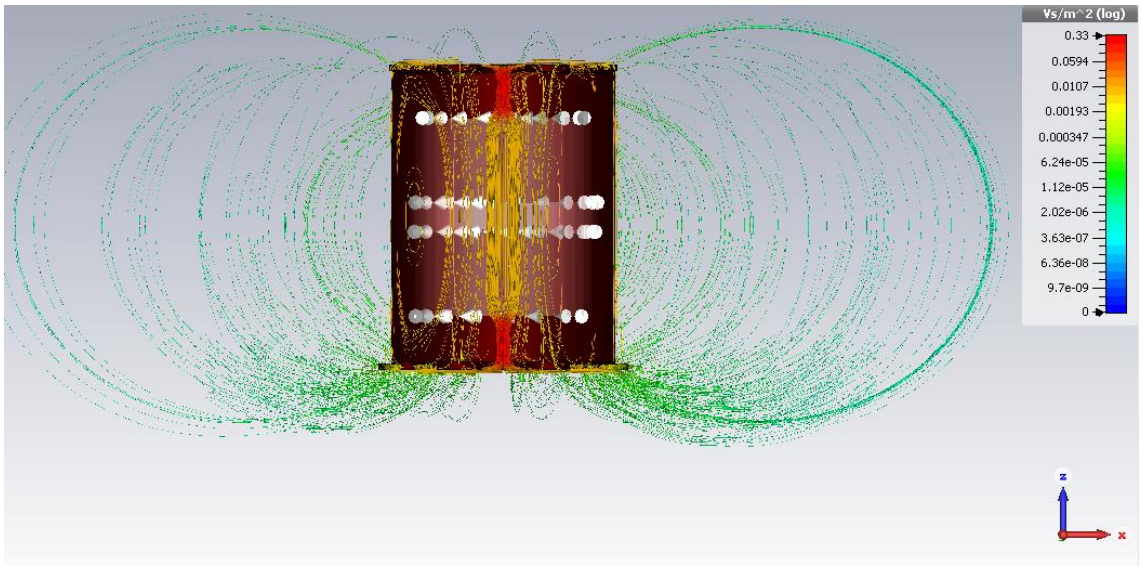

Figure 3.12: Field distribution around the storage magnet.

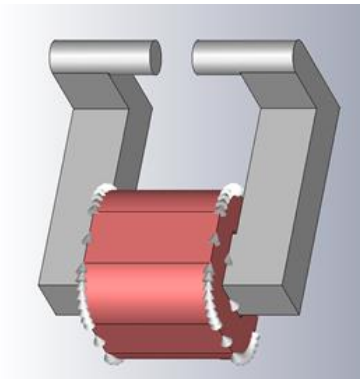

Figure 3.14: Second dipole magnet to compensate field leakage from storage magnet.

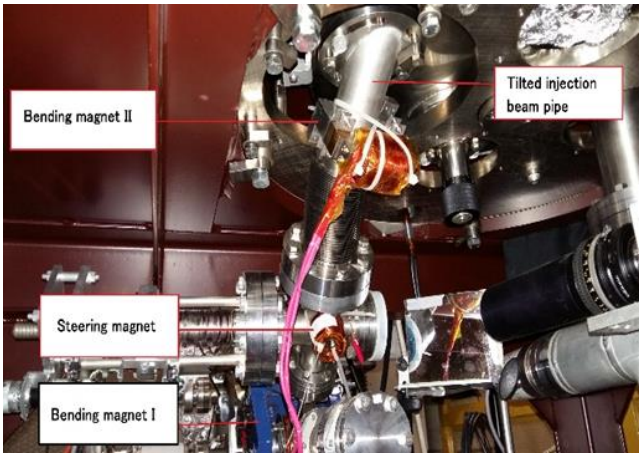

Figure 3.13: Additional bending magnet on the injection pipe of storage chamber.

3.2.3 Alignment Stage for the Storage Magnet

In order to align the storage magnet with respect to the straight beam line an alignment stage has been installed beneath the storage magnet. The alignment stage is able move the storage magnet 2 mm in left and right and also in up and down stream directions.

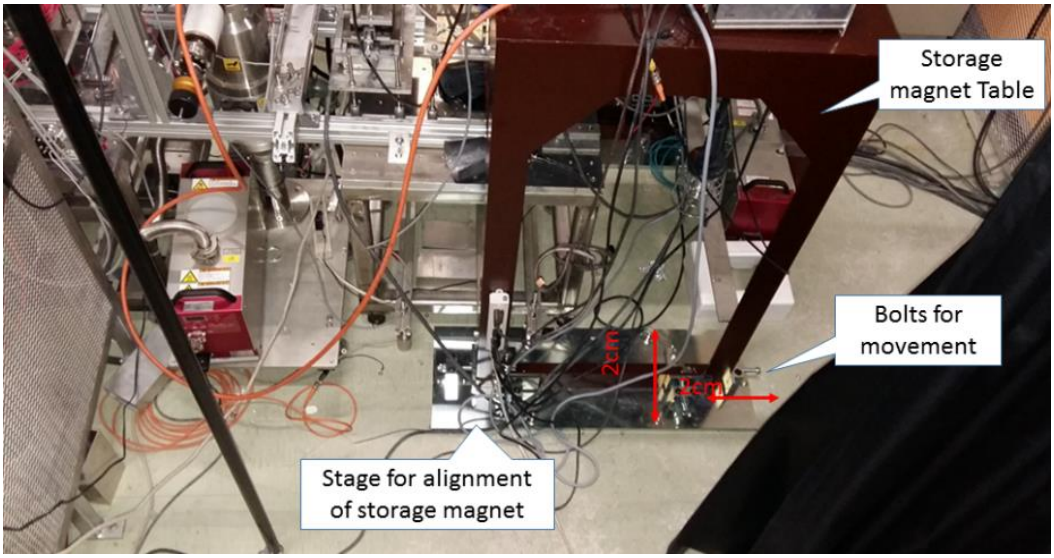

Figure 3.15: Alignment stage for the storage magnet.

3.2.4 Polarity of the Storage Magnet Auxiliary Coil

Auxiliary coil is mounted on the main coil of storage magnet to provide weak focusing in the median plane. The polarity of the auxiliary coil should be opposite to the polarity of main coil in order to provide weak focusing in the median plane. For many early trials of beam injection into the storage magnet the polarity of the auxiliary coil was wrong (polarity of main coil and auxiliary coil was same). The wrong polarity of auxiliary coil changes the required field profile at the center of the storage magnet. Fortunately, during the inspection of the storage magnet power supplies, we found the problem of the wrong polarity and fixed it.

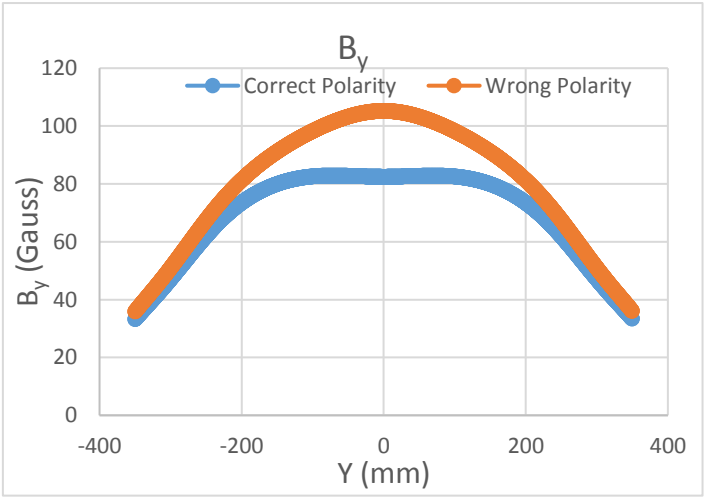

Figure 3.16: Axial field profile of (B_y) of storage magnet. Orange is showing the field profile with wrong polarity and blue is correspond to correct polarity of auxiliary coil.

Figure 3.16 and 3.17 are axial and radial field profile from CST-EM simulation. Red curves are correspond to the field profile at the wrong polarity of auxiliary coil while blue curves represent filed profile at correct polarity.

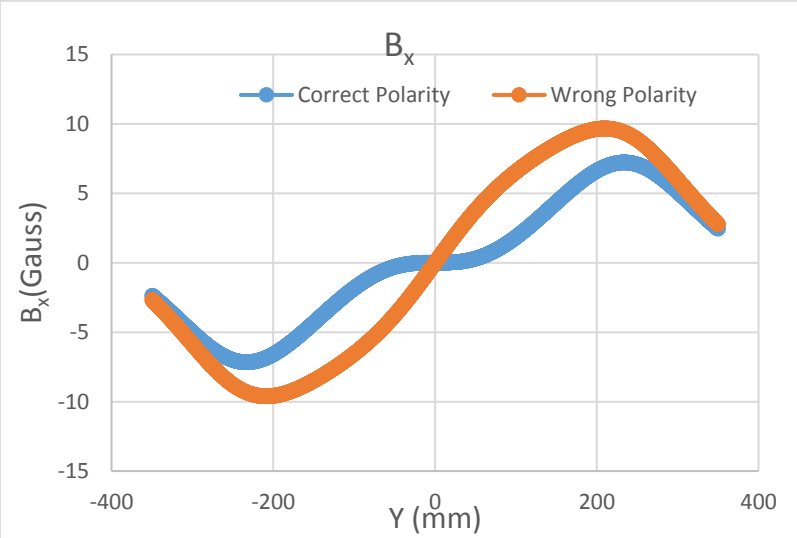

Figure 3.17: Radial field profile. Orange correspond to wrong polarity and blue is with correct polarity of auxiliary coil.

3.3 Beam Monitors in the Storage Magnet

In the first stage of the SITE two kinds of beam diagnostic monitors have been used in storage magnet 1) Interceptive fluorescent screen monitor to detect vertical positon of beam 2) Non-interceptive beam induced fluorescence monitors to observe beam track in N_2 gas. In this section beam monitoring for the first stage of SITE in the storage magnet will be discussed in detail.

3.3.1 Interceptive Monitor in the Storage Magnet

To find the vertical positon of beam inside storage magnet FS monitor had been attached to the vacuum linear feedthrough. Linear feedthrough can move fluorescent screen position vertically up and down. A mirror was positioned in front of FS to reflect light from FS to the CCD-camera (Hamamatsu-C5985). Mirror angle was adjustable form the outside to span complete vertical positon of fluorescent screen. Schematic view of this setup is depicted in Fig. 3.18.

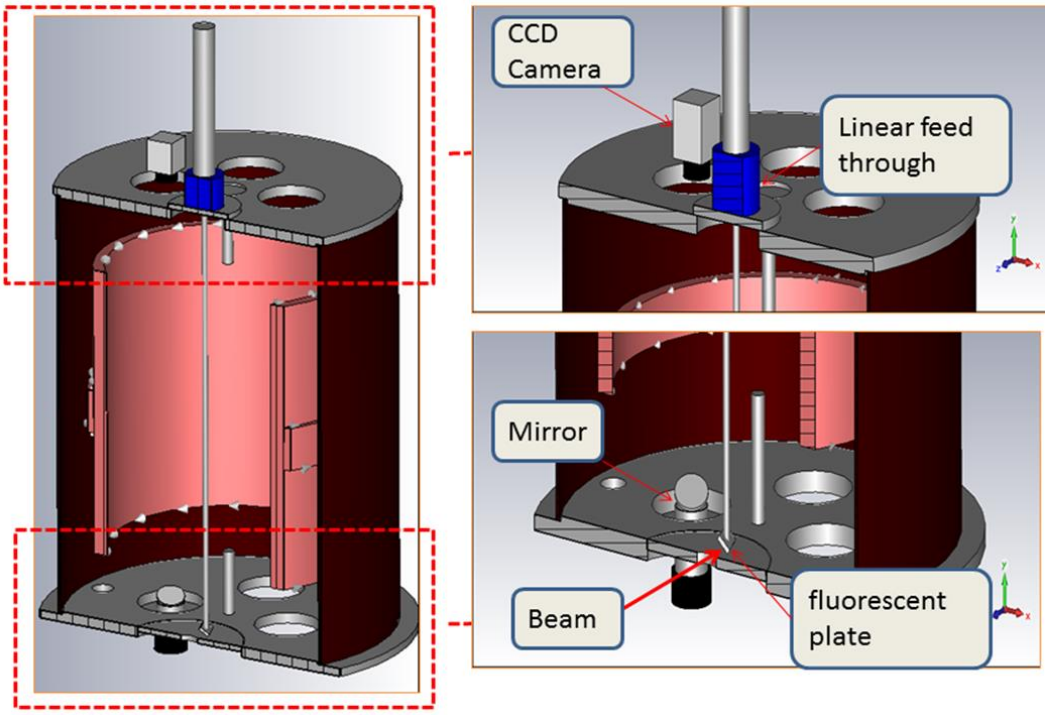

Figure 3.18: Schematic view of fluorescent screen monitor to detect vertical position of beam in storage magnet.

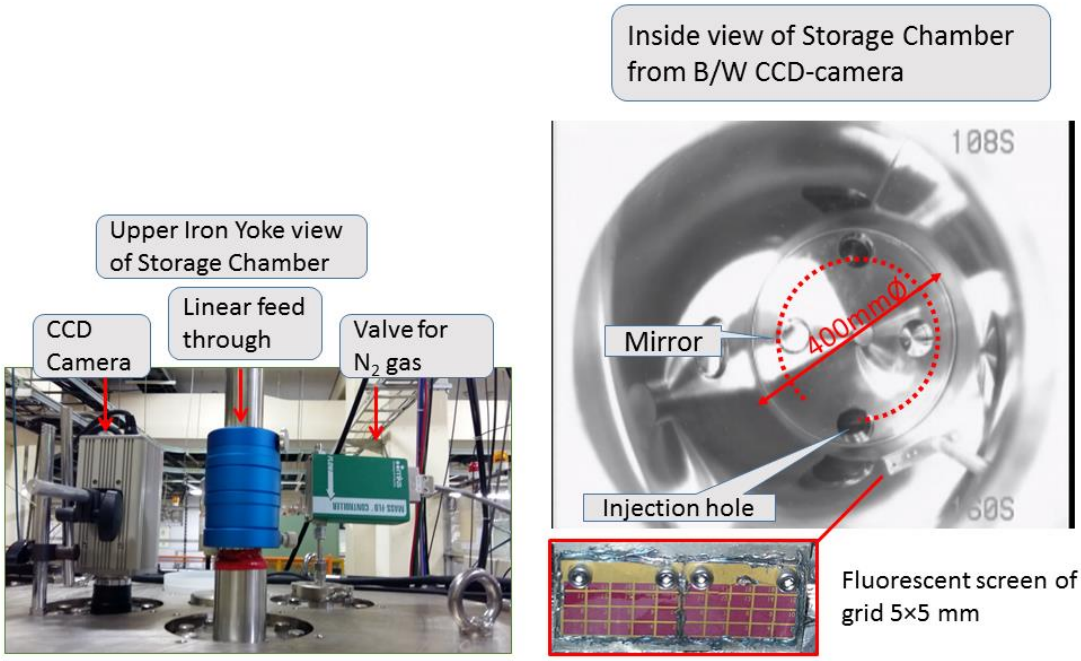

Figure 3.19: Left: Upper Iron yoke view of storage magnet which consist of CCD-camera, linear feedthrough and valve for N_2 gas. Right: Inside view of storage magnet from B/W CCD camera.

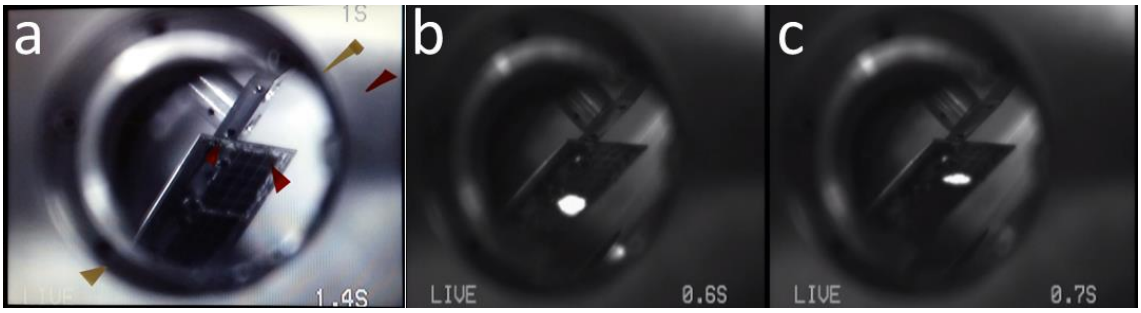

Figure 3.20: (a) Image of fluorescent screen in mirror viewed by CCD-camera without beam. (b) Beam spot at fluorescent plate in the absence of magnetic flied of storage magnet. (c) Beam spot in the presence of magnetic field of storage magnet.

Figure 3.19 is the representation of experimental setup of monitors in storage magnet. Figure 3.20 (a) is the image of fluorescent plate from CCD-camera without beam. Figure 3.20 (b) and (c) represent beam profile at FS without and with the presence of magnetic field in the storage magnet respectively. In the presence of the magnetic field beam deflect around 1 cm on FS radially which is in agreement with CST-PS tracking results.

3.3.2 Non-interceptive Monitor in the Storage Magnet

Conventional intercepting monitors are not applicable to observe the electron beam track in the storage magnet. Non-interceptive beam monitoring in the storage magnet to detect electron beam track is a challenging task due to the mechanical constraint of the storage magnet geometry. To detect electron beam track in the storage magnet non-destructively fluorescent light due to the introduced nitrogen gas has been detected by using a CCD-camera. In this section the working principle of the gas monitor will be described and after that results of nitrogen gas monitors from the storage magnet will be presented.

3.3.2.1 Working Principle

When the charge particles collides with the residual gas or specially introduced gas,

the molecules of gas are not only ionized, but also excitation of internal energy levels can occur. The excitations of gas decay electromagnetically by the emission of fluorescence light. The excitation of N_2 gas results in a transition spectrum in the optical region. The spectrum is originated by the decay of molecular ions N^+_2 excited by the collision with the beam ions in the wavelength range 390 nm < λ < 470 nm.

In high vacuum the most prominent vacuum constituent is nitrogen gas. N_2 gas pressure can be increased by the help of regulated gas valve in case of low signal strength. The fluorescence light can be monitored by a CCD or CMOS camera [21, 23, 24].

3.3.2.2 Setup

As depicted in Fig. 3.19 (a) non-invasive nitrogen gas monitor setup consist of MKS N_2 regulated valve [25] and Hamamatsu CCD camera model C5985 [26]. All of these devices were located outside of the storage magnet. The regulated valve is a general purpose mass flow controller valve from MKS instrument and used to fill the storage magnet with N_2 gas in controlled manner. By the use of the controlled valve storage magnet's vacuum chamber pressure was maintained to 1.5×10^{-3} mbar.

Hamamatsu 5985 high resolution chilled CCD camera is used to capture fluorescence light from storage chamber. The B/W Chilled CCD camera features high-sensitivity under faint light conditions, which are difficult to achieve with conventional B/W CCD cameras. Exposures time is 1/10,000 sec to 300 sec and spectral response is 400 to 700 nm [26].

3.4 Experimental Results of the Non-interceptive Monitor

The electron beam has been injected into the storage magnet with several different injection angles and was observed with a non-interceptive gas monitor. In this section, different injection angle studies and electron beam visualization results from the gas

monitor will be described in detail.

3.4.1 Electron Beam Injection at Lower Injection Angle

In order to find the correct injection angle for the injection of the electron beam into the storage magnet, injection study has been performed with several different injection angles. Injection angle of the electron beam was varied with the help of the two dipole magnets. Particle tracking in CST-PS also has been done in order to understand the experimental results. Firstly beam injection was performed at the lower angle, which results in beam hit at the lower plate of the vacuum chamber of storage magnet. Figure 3.21 represents the single particle tracking in CST-PS when the beam was injected into the storage chamber at the lower angle. In the Fig. 3.21 (a - d) injection angles were varied from 42.0^{o}, 42.5^{o}, 43.0^{o} and 43.5^{o} respectively. At these angles beam hit at the vacuum chamber of the storage magnet. When the injection angle was increased in the steps of 0.5^{o} beam hit position advanced on the vacuum chamber base plate. Figure 3.22 (a – d) are the experimental results from the gas monitor of the storage magnet. False colors are added to the original Black and White images for better visibility. Figure 3.22 (a - d) represents the case when the electron beam was injected in the storage magnet at the injection angle about 42.0^{o} by the help of main dipole magnet. Small variation in the range of 0.5^{o} were introduced by the help of the second dipole magnet. It is evident from the Fig. 3.22 (a – d) as the injection angle increases beam hit position advanced on the lower plate of the vacuum chamber.

Reflection from the Storage Magnet Vacuum Chamber:

Reflection from the chamber walls and from lower the base plate is the cause of unwanted light background in Fig. 3.22. In order to observe beam more clearly it is planned to blacken the chamber walls in order to avoid the light reflection. Detail of this plan will

be described in the next section.

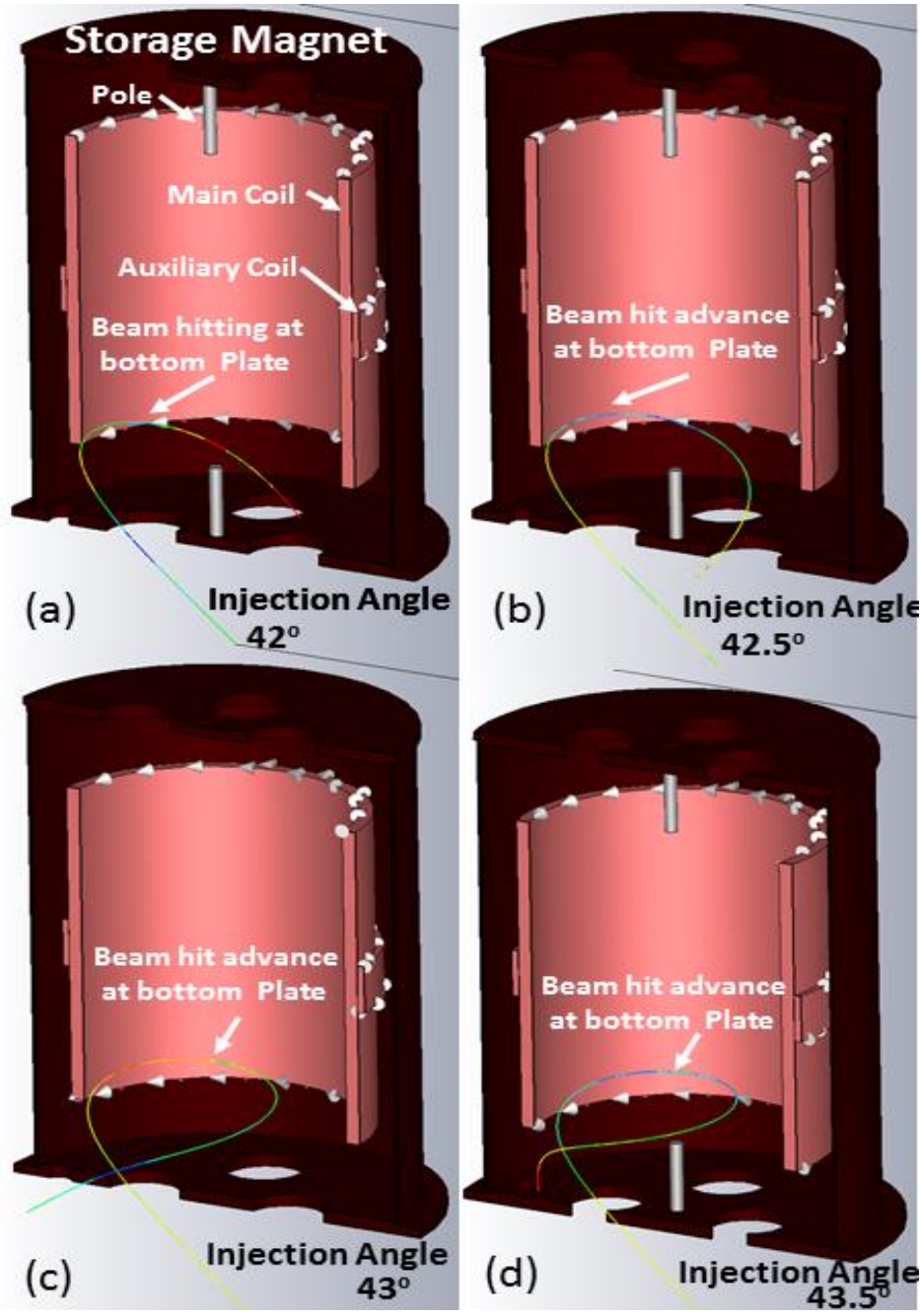

Figure 3.21: Single particle tracking in CST-PS at the different lower injection angle, (a - b) are correspond to the injection angle of 42°, 42.5°, 43°, 43.5° respectively. As injection angle increased beam hit advanced on the vacuum chamber of the storage magnet.

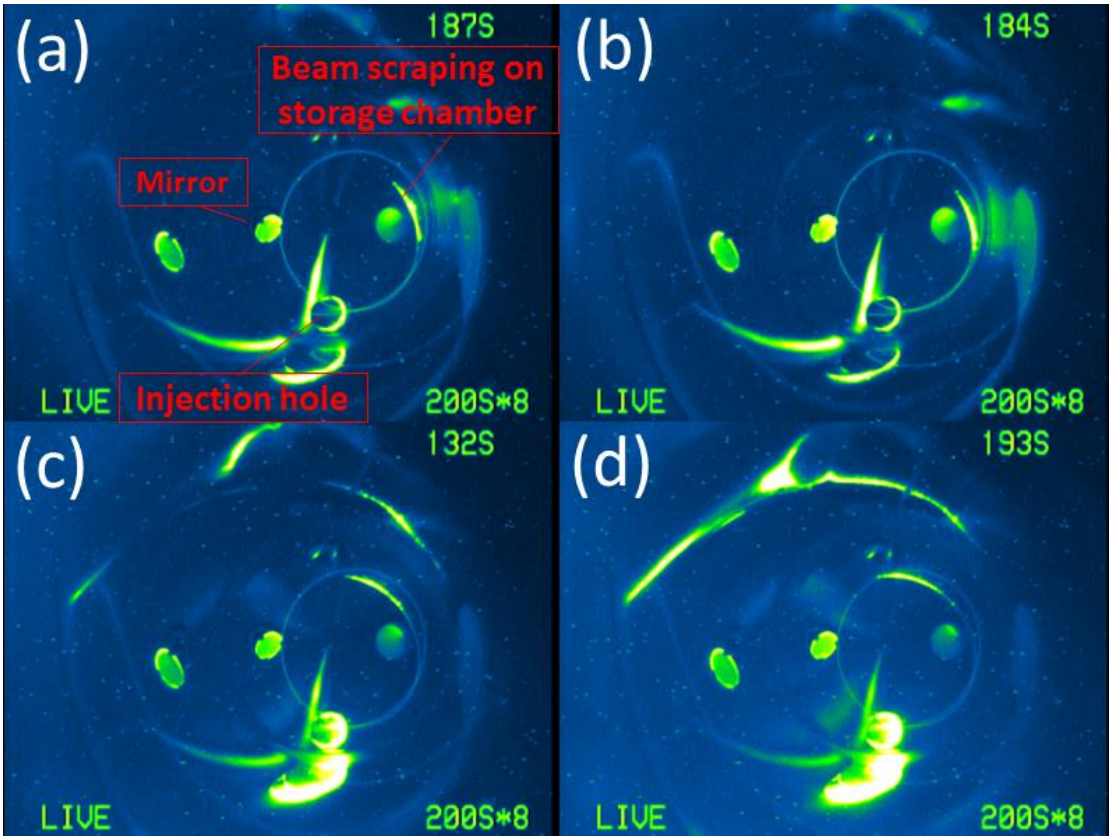

Figure 3.22: Gas monitor results from the storage magnet. The electron beam was injected into the storage magnet at 42°. Small variations in the range of 0.5° were introduced by the help of the second dipole magnet. (a - d) are correspond to the cases when the injection angles were increased up to 43.5°. (False colors are to the original B/W pictures for the better visibility)

As the injection angle increased the pitch distance between two turns also increase.

3.4.1 Electron Beam Injection at Higher Injection Angle:

In the next step, the electron beam injection was performed at the higher injection angle in the storage magnet. Figure 3.23 represents the particle tracking in CST-PS at the higher injection angle. In Fig. 3.23 (a - f) beam was injected into the storage magnet at 44°, 44.5°, 45°, 45.5°, 46°, 46.5°, 47° respectively. Only two turns appear at those higher angle.

Figure 3.24 is the representation of the experimental situation when the electron beam was injected into the storage magnet at the injection angle 44° by using the main dipole magnet and variations in the injection angles were introduced by the help of the second

dipole magnet. Figure 3.24 (a – f) shows the case when the injection angle was increased in the steps of 0.5^{o} up to 47^{o}. Figure 3.23 and 3.24 are not perfect one to one correspondence and view of observing trajectory in both figures is also different.

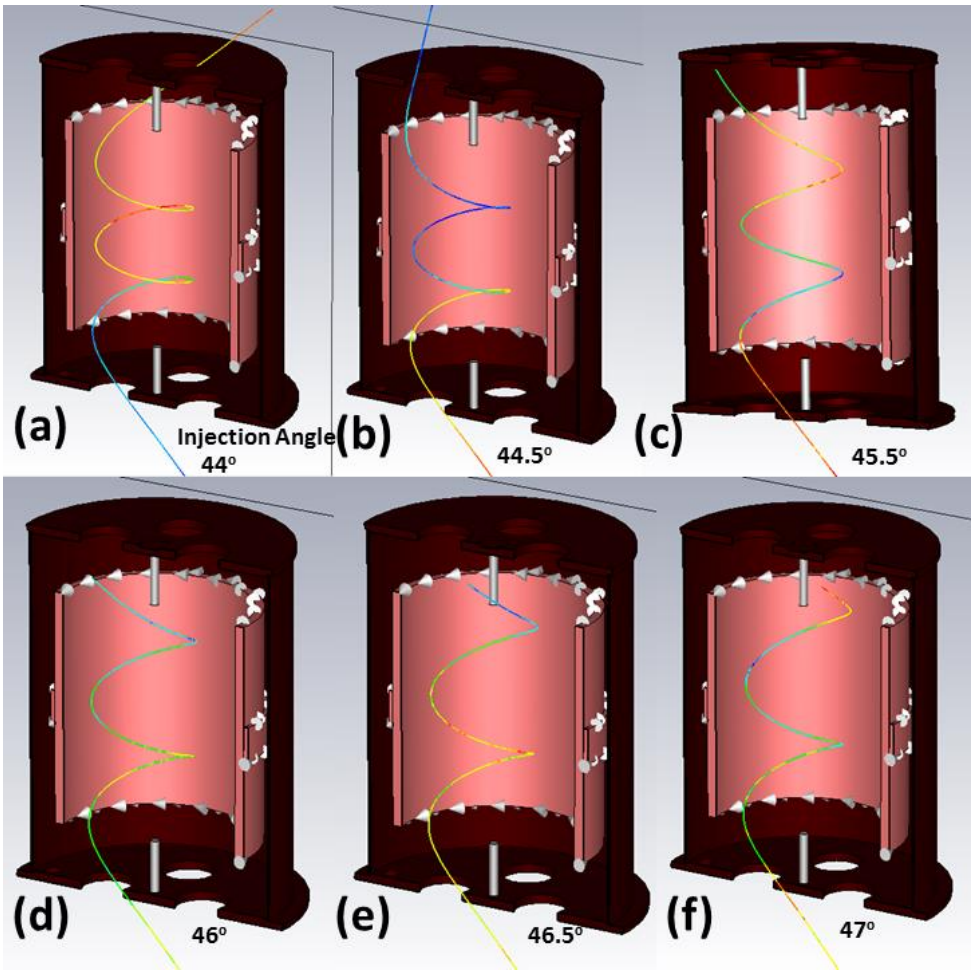

Figure 3.23: Single particle tracking in CST-PS at the different high injection angle, (a - f) are correspond to the injection angle of 44^{o}, 44.5^{o}, 45^{o}, 46^{o}, 46.5^{o}, 47^{o}, respectively. Only two turns are visible at those higher injection angles. As injection angle increase distance between these two turns also increase.

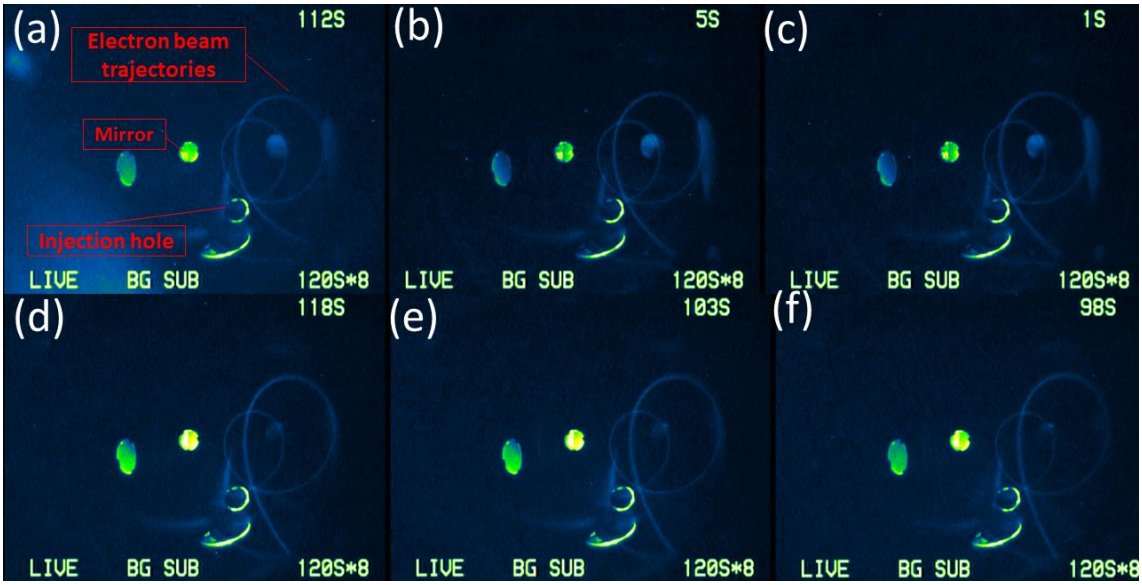

Figure 3.24: Beam injection into the storage magnet at the higher injection angles. Injection angle was 44^{o} from the main dipole magnet and small variations in the injection angles were introduced by using the second dipole magnet. (a -f) are the case when the injection angles were increased in the steps of 0.5^{o} up to 47^{o}. (False colors are to the original B/W pictures for the better visibility)

3.4.1 Electron Beam Injection at (43.5^{o} < injection angle < 44^{o})

After performing the above mentioned injection angle studies, electron beam was injected into the storage magnet in the angle range of 43.5^{o} < injection angle < 44^{o}. Particle tracking study in this injection angle range in CST-PS is shown in Fig. 3.25, this injection angle is correspond to multi turns injection. Figure 3.26 is the picture from the gas monitor of the storage magnet, when the electron beam was injected into the storage magnet at the angle greater than 43.5^{o} and less than 44^{o} (43.5^{o} < injection angle < 44^{o}). In the Fig. 3.26 the first turn of the electron beam appear clearly but after completing first turn beam start diverging. Although the reference trajectory is present but as a collectively beam lost its intensity and we cannot observe the beam as fluorescent light from the gas monitor.

As explained in the section 3.3.1, FS monitor was installed in the storage magnet in order to detect the vertical position of the electron beam. In the case of injection angle

(43.5° < injection angle < 44°), beam hit at the FS monitor at its maximum position was still observed even we lost beam after the first turn. Beam lost its intensity but some trajectories goes up to the top of the storage magnet. Therefore, some part of beam hit at the FS monitor in the case of defocusing too.

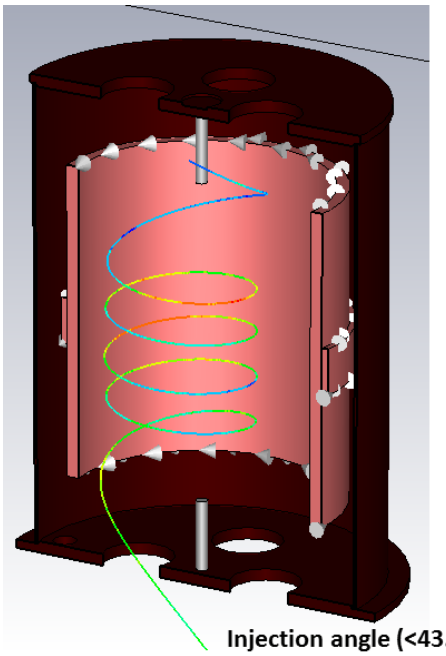

Figure 3.25: Single particle tracking in the storage magnet at the angle 43.5°.

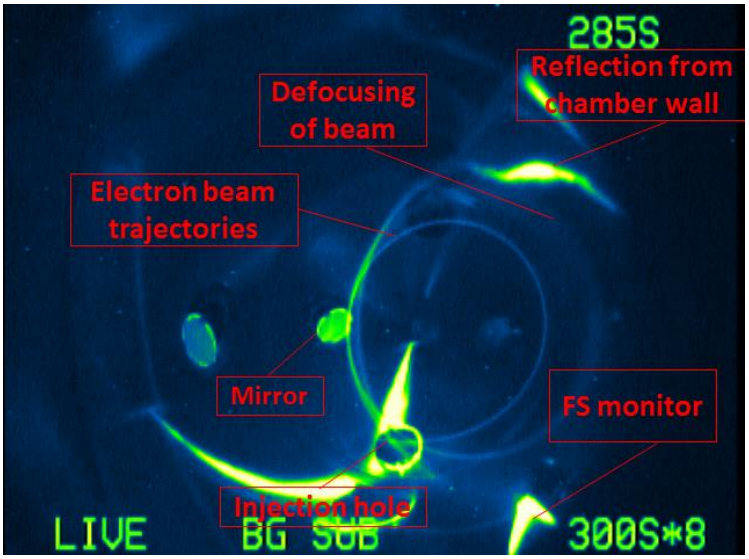

Figure 3.26: The electron beam injection into the storage magnet at the angle greater than 43.5° and less than 44° (43.5° < injection angle < 44°).

3.5 Defocusing of the Electron Beam in the Storage Magnet

Figure 3.25 is the case of single particle tracking in CST-PS when the electron beam was injected into the storage magnet at the injection angle greater than 43.5° and less than 44° (43.5° < injection angle < 44°), in this case multi turns appeared in the storage magnet. But multi turns were not observed in the experiment. Therefore, multi particle tracking with 500 particles also had been performed to understand the situation and it was found that the electron beam start diverging after the first turn in the case of multi particle beam. Figure 3.27 (b) is the multi particle tracking in the storage magnet, it evident from the Fig. 3.27 (b) that beam start diverging after completing the first turn. Defocusing of the beam happens due to the particular shape of the radial field profile of the storage magnet. Radial field of the storage magnet varies very rapidly along the axial position of the storage magnet, thus electron beam of finite size at different vertical positions experience different radial field and hence take different path in the storage magnet. Radial field profile of the storage magnet and its derivative are shown in Fig. 3.28 left and right.

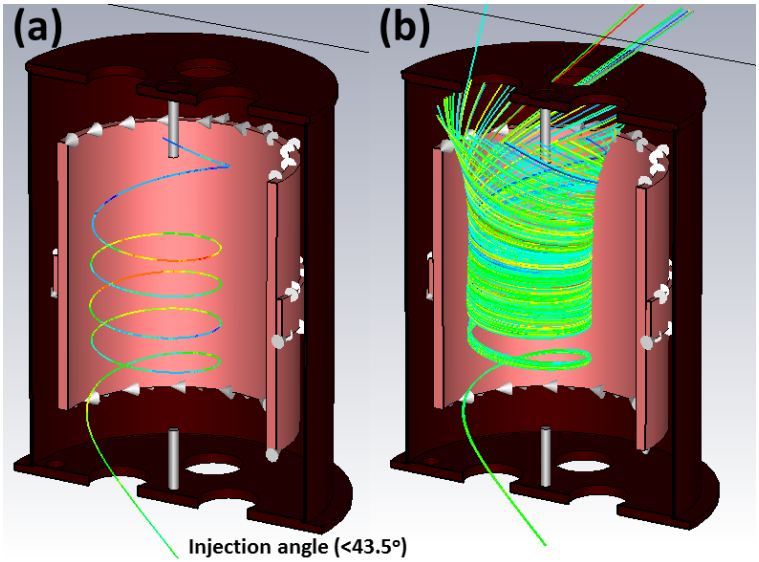

Figure 3.27: (a) At the injection angle greater than 43.5 and less 44° (43.5° < injection angle < 44°) multi turns appears. (b) Multi particle tracking in the storage magnet shows defocusing of electron beam the storage magnet.

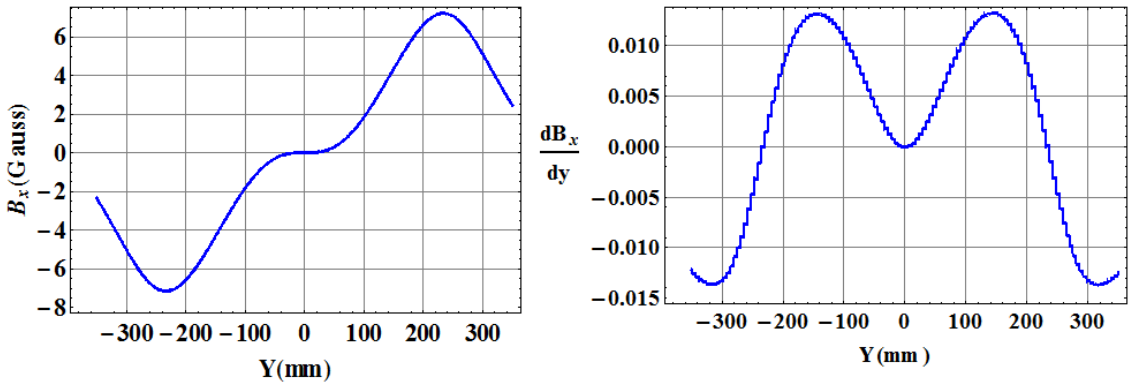

Figure 3.28: Left: Radial field profile of the storage magnet. Right: is the derivative of radial filed profile with respect to the solenoidal axis of the storage magnet.

3.6 Solution for Defocusing of the Electron Beam

In order to solve defocusing of the electron beam in the storage magnet Twiss parameters at the injection point are needed to be controlled. Reverse tracking with finite size distribution of the electron beam from the center of the storage magnet has been performed in CST-PS to estimate the required Twiss parameters at the injection point.

Radial field of the storage magnet varies rapidly axially in the storage magnet but in radial direction it do not change much. Therefore, particle distribution of length 1 mm (11 particles) radially with no vertical distribution has been assumed. Figure 3.29 represent the assumed distribution of particles at the distance of 120 mm radially from the center of the storage magnets. Particle tracking in 3-D coordinates are shown in Fig. 3.30.

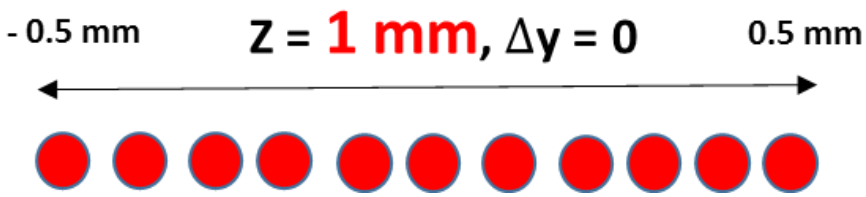

Figure 3.29: Assumed particle distribution at the radius 120 mm in the storage magnet.

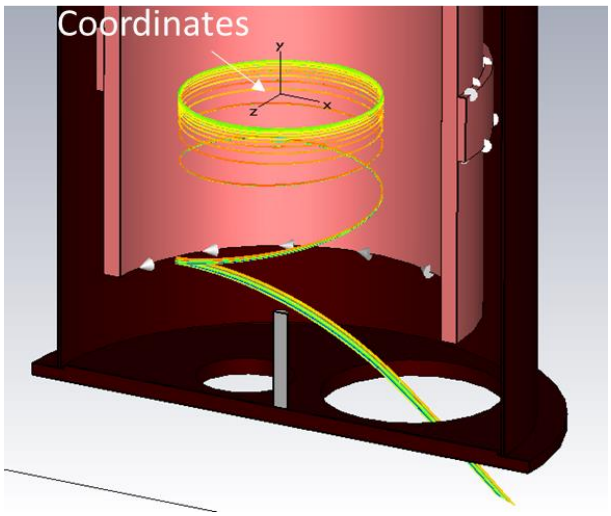

Figure 3.30: Multi-Particle tracking in the storage magnet.

Figure 3.31 shows the particle tracking in x-y vertical plane and x-z radial plane of the storage magnet. Black circle in the Fig. 3.31 right shows the required beam at the injection point of the storage magnet. Figure 3.32 shows the phase space of the required beam at the injection point. Table 3.1 summarize the required emittance and Twiss parameters of the beam in both transverse direction (x-z).

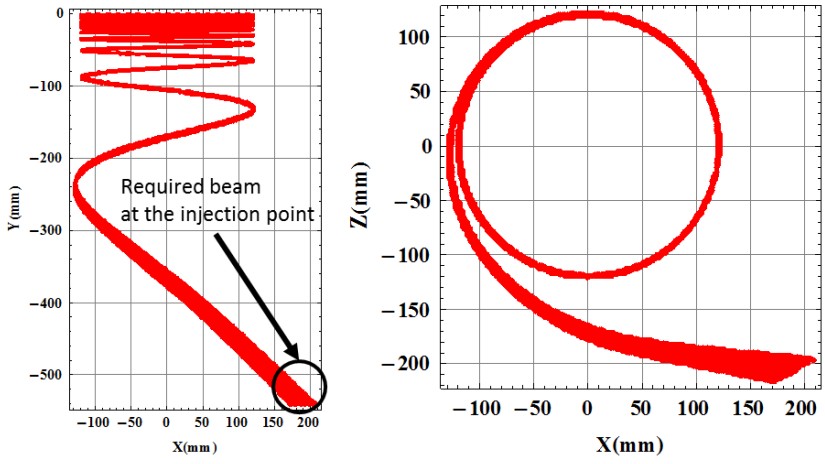

Figure 3.31: Left: Multi-Particle tracking in the x-y plane of the storage magnet. Black circle represent the required beam shape at the injection point. Right: Particle tracking plot in the x-z plane.

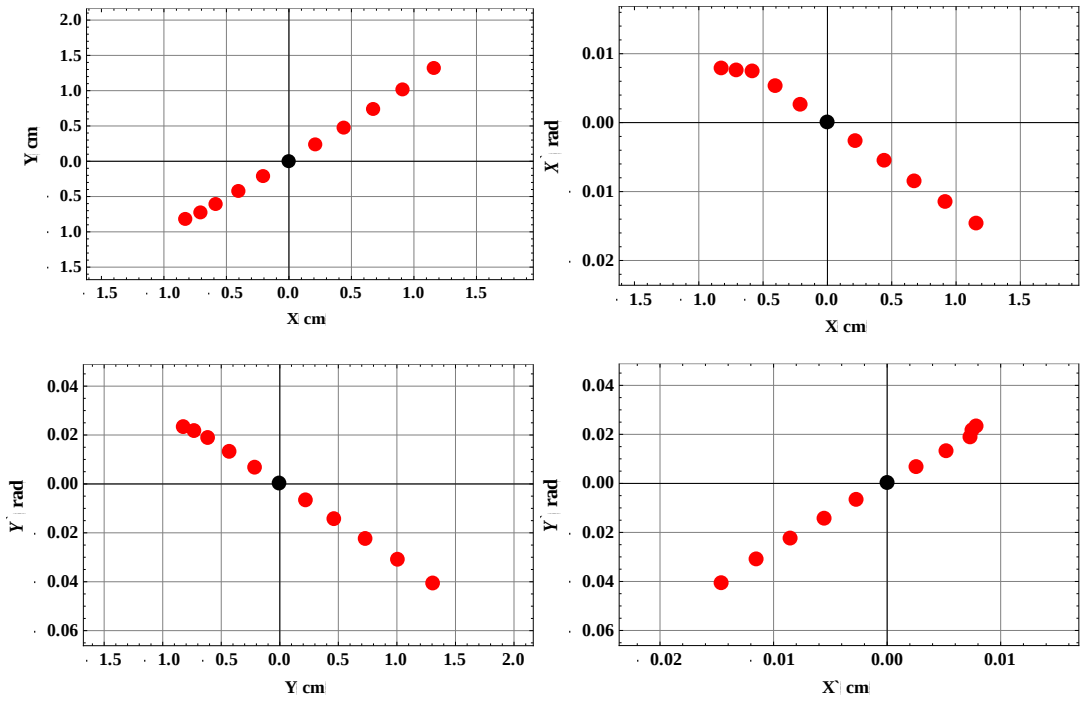

Figure 3.32: Phase space plots of the required beam at the injection point. Black point represent the reference trajectory.

Small emittance and straight beam is required at the injection point in order to overcome the defocusing of the beam in the storage magnet. Quadrupole magnets are needed to create required beam at the injection point. Simulation in SAD (Strategic Accelerator Design) will be carried out to estimate the required number of quadrupoles magnets and their specifications.

Table 3.1: Twiss parameters at the injection point of the storage magnet.

Twiss Parameters	Values
ϵ_x	$4.24 \times 10^{-6}\ m\ rad$
β_x	9.75
α_x	11.61
ϵ_y	4.01×10-6 *m rad*
β_y	11.95
α_y	36.31

3.7 Future Plans

In the second stage of SITE, two major development are planned to complete

- Magnetic kicker system to kick electron pulses to the median plane
- Beam monitors

3.7.1 Reflection from Chamber Walls

Base plate of storage chamber and walls pose good reflective properties. Reflection of fluorescent light from chamber is source of background in the pictures from gas monitors, it is plan to blacken chamber wall to avoid light reflection.

Two option are under consideration

- Graphite powder solved in Isopropanol (Aerodag g) [29]
- Light Exclusion Sheet Super Black from SHIBUYA OPTICAL CO.,LTD [30]

3.7.2 Magnetic Kicker

Kicker coils will be used to kick the electron pulses at appropriate position in storage magnet and direct it to median plane (storage region). After kick “pitch angle” (vertical momentum) of electron pulses will become zero and finally electron pulses will be stored in the storage region. Detail design and simulation study for the fabrication of kicker coil system will be done in second stage of SITE. To accumulate electron beam, effectively, a pulsed kicker should fire coincide with electron beam. Careful tuning works of timing and kick power is required.

Followings are the major tasks associated with kicker system

- Simulation and fabrication of kicker coils.
- Design and fabrication of kicker coil’s pulsed current power supply.
- Trigger control system to fire pulse kicker coincide with electron pulses.

- Beam tracking studies in the presence of kicker coils for successful storage of beam.

Development and verification of this kicker system with electron beam is directly related to the success of actual experiment's kicker system. Understanding the operation of this novel kicker system for test experiment may reduce trial operation cost of J-PARC muon g - 2/EDM experiment.

3.7.3 Beam Monitors:

Currently we are utilizing fluorescent plate and fluorescence light from N_2 gas excitation to detect electron beam inside storage magnet.

Due to the high voltage of kicker system gas monitor is not applicable after the installment of the kicker system. N_2 gas will also not provide any information about the stored beam. One possible candidate for non-interceptive beam monitor is the installation of two metal plates namely "pick-up plates" at the median plane of the storage magnet. The measurement of induced electric field of electron pulses on these metal plates can provide us information about the stored beam too.

Chapter 4

Summary and Conclusions

Three-dimensional spiral injection is one of a key idea for the new J-PARC muon *g* – 2/EDM experiment. For the establishment of this novel scheme, the Spiral Injection Test Experiment (SITE) by the use of the electron beam is under development at KEK Tsukuba campus. SITE is divided into two stages. The first stage goal is to detect a DC electron beam spiral track in the storage magnet as fluorescent light from nitrogen gas excitation along the electron beam path. The second stage and final goal is to store pulsed electron beam for the order of milliseconds. In the first stage of SITE, 80-keV thermionic electron gun has been installed to produce the electron beam. A 2-m long beamline has been constructed to transport an electron beam from an electron gun to the storage magnet. Simulation study of straight beam line components has been carried out in CST-PS. At three different locations on straight beam line fluorescent screen (FS) monitors have been placed and beam profiles at those locations were confirmed. Each component of beam line was described in detail.

Beam commissioning from straight beam line to the storage magnet has been done with the help of five pairs of steering magnets and one main dipole magnet. The main dipole magnet is one of the most important component in this experiment and used for injection of the electron beam from the straight beam line into the storage magnet. Field measurement of the dipole magnet has been done at a typical current value of 2.79 A which corresponds to the field strength of 125 gauss and the effective length of dipole magnet is estimated 59.4 mm which deflect electron beam at 43degree.

A solenoidal storage magnet has been designed, simulated and constructed. The storage

magnet for SITE represents all important features as in the E34 storage magnet. An auxiliary coil is mounted on the center of the main solenoidal coil to provide weak focusing in the storage region. Field measurement of the storage magnet has been performed at the main coil current 8 A and different auxiliary coil currents (0 A, 2.2 A, 4.3 A, 6.5 A, 8.7 A, 10 A) with the uncertainty of 1 gauss.

Several challenges have to overcome during the beam commissioning into the storage magnet. Some of them are summarized here.

1) During the electron beam commissioning from straight beam line to the storage magnet, it was found that due to the particular shape of beam pipe (bellows on both ends of pipes: which makes it bend in the center region) beam hit at injection pipe. After confirming beam hit by the thermal camera, injection pipe has been replaced with appropriate beam pipe (bellows in downstream direction replaced with straight pipe). After replacing injection pipe electron beam has been confirmed in the storage magnet by FS monitors.

2) For the alignment of the storage magnet with respect to the straight beam line an alignment stage also has been installed.

3) For the initial trials of beam injection into the storage magnet polarity of the auxiliary coil of the storage magnet was wrong. Due to which, injection was not completely successful. After the inspection of power supplies for the storage magnet, polarity of auxiliary has been fixed.

4) Due to the field leakage from the storage magnet injection hole, injected beam couldn’t enter into the storage magnet at the designed angle. After detecting this problem additional bending magnet has been installed at the injection pipe to overcome the field leakage effect.

Storage chamber was filled with N_2 gas to observe the electron beam in non-interceptive way due to the emission of fluorescent light from the nitrogen gas excitation. 80 keV electron beam in the storage magnet of 83 gauss field with the diameter of 24 cm has been captured as fluorescent light by using Charge Coupled Device (CCD)-camera.

In order to understand the effect of injection angle on beam trajectory in the storage magnet, the injection angle of the electron beam was varied and its effect on beam track were observed.

Furthermore, it was identified that the electron beam vertically defocused due to the radial field of the storage magnet. Due to vertical defocusing of electron beam, only two turns were observed clearly. In the next step, Twiss parameters at the injection region will be controlled in order to solve vertical defocusing of the beam in the storage magnet.

In the first stage of SITE, the experimental setup was built successfully and through many systematic studies, the optimal conditions for experiment has been determined. The goal of the first stage to detect electron beam track as a fluorescent light was achieved.

For the second stage of SITE, electric chopper system to produce pulsed beam was designed, simulated and fabricated to produce electron beam of pulse length of 50 ns. The mechanical design and electrical parameters of electric chopper system were described in detailed. Electric chopper system is almost ready to be installed on the beam line.

In the second stage the magnetic kicker coil system will be installed in order to guide electron beam pulses to the very center of the storage magnet. Beam monitors also need to be improved to confirm the storage of the beam. The second stage goal is to store electron beam pulses for the order of milliseconds to prove the concept of newly developed spiral injection scheme.

References:

[1] G.W. Bennet *et al*., "Final Report of the muon E821 anomalous magnetic moment measurement at BNL", Phy. Rev D 73 (2006) 072003

[2] H. Ando *et al*., "Technical Design Report for the Measurement of the Muon Anomalous and Electric Dipole Moment at J-PARC", unpublished

[3] J. Bailey *et al.*, "Final report on the cern muon storage ring including the anomalous magnetic moment and the electric dipole moment of the muon, and a direct test of relativistic time dilation", Nucl. Phys. B 150 (1979)

[4] P. Bakule *et al*., "Measurement of muonium emission from silica aerogel", Prog. Thero. Exp. Phy. (2013) 103C01

[5] G.A. Beer *et al*., "Enhancement of muonium emission rate from silica aerogel with a laser ablated surface", Prog. Theor. Exp. Phys. 2014 (2014) 091C01,

[6] H. Iinuma, H. Nakayama *et al.*, "Three-dimensional spiral injection scheme for the g-2/EDM experiment at J-PARC", Nucl. Instrum. Meth, Vol. A832, pp. 51-62 (2016).

[7] A.Yamamoto *et al.*, "The super conducting inflector for the BNL *g* - 2 experiment", Nucl. Instrum. Methods Phys. Res. Sect. A 491 (2002) 23–40,

[8] J. D. Jackson, Classical Electrodynamics, Second Edition (John Wiley & Sons, New York, 1975).

[9] S. Ohsawa *et al.*, "Performance of an electron gun for a high-brightness X-ray generator", J. Synchrotron Rad. (2008). 15, 258–261

[10] C. Wall, R. Levine, "*Physics laboratory manual"*, Prentice-hall, Inc. (1962).

[11] S. Brody, S. Singer, "Experiment on thermionic emission of electrons*"*, Amer. J. Phys. 38.

[12] H. A. Jones, I. Langmuir, “The characteristics of tungsten filaments as functions of temperature”, GE Rev., vol. 30, pp. 354-361 (1927).

[13] http://www.cst.com

[14] Electron Optics (Second Edition) by P. Grivet, P. W. Hawkes and A. Septier
ISBN: 978-0-08-016226-3

[15] https://www.trifield.com/content/vector-magnitude-gaussmeter-model-vgm/

[16] http://www.opera.com

[17] www.matsusada.com/

[18] Agilent 81101A http://www.keysight.com/en/pd-1000001729%3Aepsg%3Apro-pn-81101A/pulse-generator-50-mhz?nid=536902328.536881944&cc=US&lc=eng

[19] PVX 4140: http://ixyscolorado.com/

[21] Lecture Notes on Beam Instrumentation and Diagnostics by Peter Forck GSI Joint University Accelerator School January – March 2011 p.42

[22] R. Jung, G. Ferioli, S. Hutchins Proc. Diag. Instrum. Part. Acc. Conf. DIPAC 03, Mainz, p. 28 (2003)

[23] http://www.wolfram.com

[24] http://https://imagej.nih.gov/ij/

[23] P. Forck, Proc. Int. Part. Acc. Conf. IPAC 10, Kyoto, p.1261 (2010)

[24] D. P. Sandoval *et al.*, Proc. Beam Instr. Workshop BIW 93, Santa Fe, p. 273 (1993)

[25] https://www.mksinst.com/product/Product.aspx?ProductID=1363

[26] http://www.spectroscopic.com/Hamamatsu/Hamamatsu_Camera_Catalog.pdf

[29] http://www.laddresearch.com/chemicals/aerodag-g

[30] http://www.shibuya-opt.co.jp/eng/super_black.html

Appendix A

Vacuum System of Muonium Production Experiment at the J-PARC 2016A

Introduction:

Systematic studies has been performed to enhance Muonium yield from different silica aerogel target at J-PARC from Jan. 14 to 16, 2017. Detail of experiment can be found in [1]. I was responsible for vacuuming of apparatus during my shit duty. In this section I will describe the procedure of vacuuming during all runs and history of vacuum during all runs. Figure A.1 is showing the apparatus of Muonium production experiment. Vacuum system is consist of following components

1) Roughing Pump (Scroll Pump)

2) Turbo Molecular Pump

3) Needle valve (VN) connected to the main chamber to control speed of pumping

4) TMP valve (VT)

5) Gate valve between TMP and Main chamber

6) Valve for roughing pump VY.

7) Pirani Gauge [Active Pirani Gauge-M (APGM)] for low vacuum 1×10^{-4} Torr.

8) Cold Cathode Gauge [Active Inverted Magnetron-M (AIMS)] for high vacuum 1×10^{-8} Torr.

9) Vacuum Monitor and Logger to record vacuum data.

Special caution is required during pumping in the presence of fragile aerogel sample. Therefore, one has to act on manual carefully in course of exchanging aerogel sample.

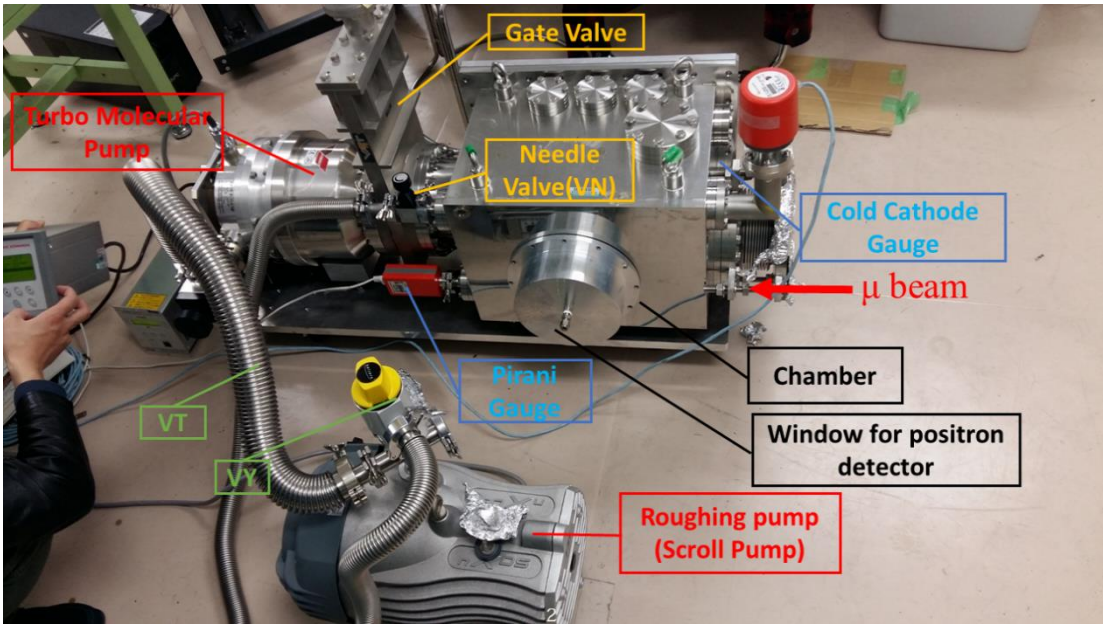

Figure A.1: Mu Production apparatus with Vacuum components labeled

Target Exchange:

During "silica aerogel target" change, one has to vent chamber first to open it and after replacement of target vacuum again to maintain required operational vacuum value. Aerogel targets are very fragile. Mishandling can easily damage targets. Fig. A.2 depicts the inside view of the chamber with a target.

Aerogel target in its box is covered with papers on both sides, during placement of target in the holder try to fit it with paper first and then remove papers from both sides. Figure A.3 is showing the aerogel target in the holder.

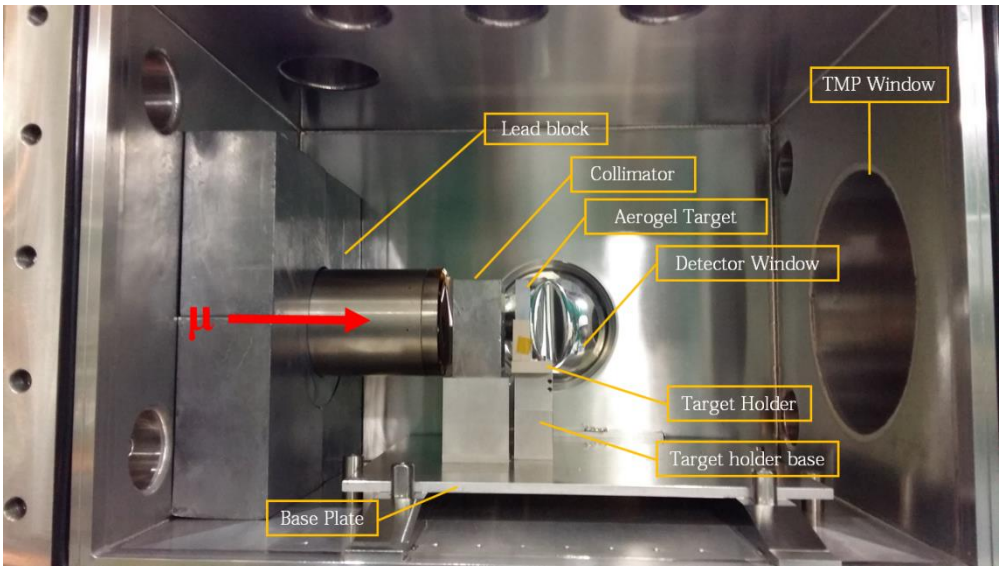

Figure A.2: Inside view of Chamber with Aerogel target

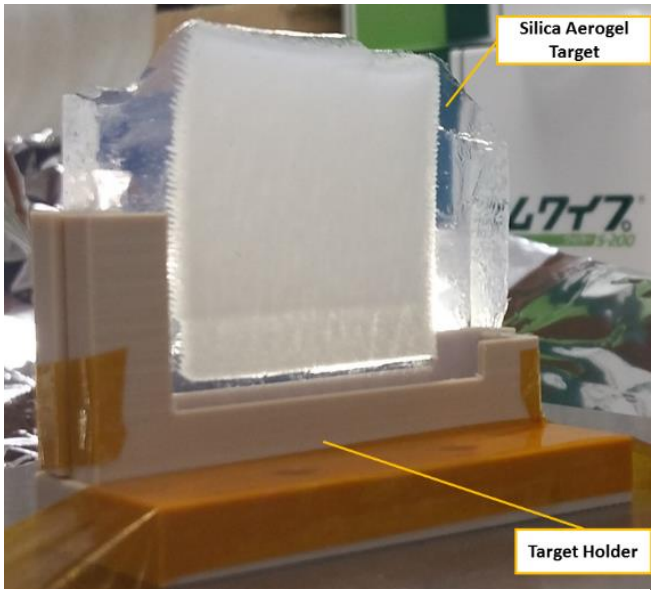

Figure A.3: Silica Aerogel target in holder

Vacuuming Procedure:

Vacuum manual is already available on run page website but for the sake of completion, vacuum procedure is discuss here too.

1. Close all valves (Gate valve, VN, VY, VT).
2. Turn ON roughing pump (Scroll pump).
3. Open VY (attached to roughing pump).

4. Slowly open VN (attached to chamber) in more than 5 minutes. Wait for 1×10^{1} Torr. Be very careful in the presence of target.

5. When pressure reach to the 1×10^{1} Torr close VY and VN.

6. Open VT (attached to TMP) completely and wait for 2 minutes.

7. Open Gate valve completely and wait for 1×10^{-1} Torr.

8. Turn ON TMP and AIMS (gauge for high vacuum) within 7 minutes it will reach to its maximum RPM 33600 and pressure ~ 2×10^{-5} Torr.

9. If not check for leak e.g tight bolts.

Procedure of Venting:

1. Close Gate valve completely.

2. Turn OFF TMP.

3. Disconnect pipe of chamber from roughing pump.

4. Slowly open VN in ~10 minutes to reach 7.6×10^{2} Torr (atmospheric pressure). Again, be careful during this step.

5. Now you are ready to open chamber.

Data logging:

During all runs, vacuum data in form of voltages was saved on midi LOGGER GL820. After the completion of the experiment, we connected the logger to the PC via LAN and copied all data. Data was in binary form we converted it into text form using GL-connection software freely available on vendor website [3]. We can also save data in text form directly on logger but first, we have to choose the extension of file.

We used AIMS (Active Inverted Magnetron-M) for high vacuum monitoring. To convert voltages into pressure I downloaded the table of conversion from vendor website [2] as shown in Fig. A.4 and write down these values in form of list into the

MATHEMATICA Then I used “interpolation” command in MATHEMATICA to construct new data points within specified data range of this data.

I added timing correspond to each run in excel file then I imported that file into MATHEMATICA and used its voltage data from CH2 as an input to “Interpolation” command and drew Log graphs corresponding to each run.

Table 2 - Pressure and voltage characteristics for nitrogen and dry air: AIM-S and AIM-SL Gauges

Pressure (mbar)	Output voltage (V)	Pressure (torr)	Pressure (mbar)	Output voltage (V)	Pressure (torr)
1.0×10^{-8}	2.00	7.5×10^{-9}	6.9×10^{-6}	6.40	5.2×10^{-6}
2.4×10^{-8}	2.50	1.8×10^{-8}	8.4×10^{-6}	6.60	6.3×10^{-6}
5.8×10^{-8}	3.00	4.4×10^{-8}	1.0×10^{-5}	6.80	7.5×10^{-6}
8.1×10^{-8}	3.20	6.1×10^{-8}	1.2×10^{-5}	7.00	9.0×10^{-6}
1.1×10^{-7}	3.40	8.3×10^{-8}	1.4×10^{-5}	7.20	1.1×10^{-5}
1.5×10^{-7}	3.60	1.1×10^{-7}	1.7×10^{-5}	7.40	1.3×10^{-5}
2.1×10^{-7}	3.80	1.6×10^{-7}	2.0×10^{-5}	7.60	1.5×10^{-5}
2.9×10^{-7}	4.00	2.2×10^{-7}	2.4×10^{-5}	7.80	1.8×10^{-5}
4.0×10^{-7}	4.20	3.0×10^{-7}	2.9×10^{-5}	8.00	2.2×10^{-5}
5.4×10^{-7}	4.40	4.1×10^{-7}	3.5×10^{-5}	8.20	2.6×10^{-5}
7.3×10^{-7}	4.60	5.5×10^{-7}	4.3×10^{-5}	8.40	3.2×10^{-5}
9.8×10^{-7}	4.80	7.4×10^{-7}	5.7×10^{-5}	8.60	4.3×10^{-5}
1.3×10^{-6}	5.00	9.8×10^{-7}	7.9×10^{-5}	8.80	5.9×10^{-5}
1.7×10^{-6}	5.20	1.3×10^{-6}	1.2×10^{-4}	9.00	9.0×10^{-5}
2.2×10^{-6}	5.40	1.7×10^{-6}	1.9×10^{-4}	9.20	1.4×10^{-4}
2.8×10^{-6}	5.60	2.1×10^{-6}	3.3×10^{-4}	9.40	2.5×10^{-4}
3.6×10^{-6}	5.80	2.7×10^{-6}	6.7×10^{-4}	9.60	5.0×10^{-4}
4.5×10^{-6}	6.00	3.4×10^{-6}	1.7×10^{-3}	9.80	1.3×10^{-3}
5.6×10^{-6}	6.20	4.2×10^{-6}	3.6×10^{-3}	9.90	2.7×10^{-3}
			1.0×10^{-2}	10.00	7.5×10^{-3}

Figure A.4: voltage to pressure conversion Table

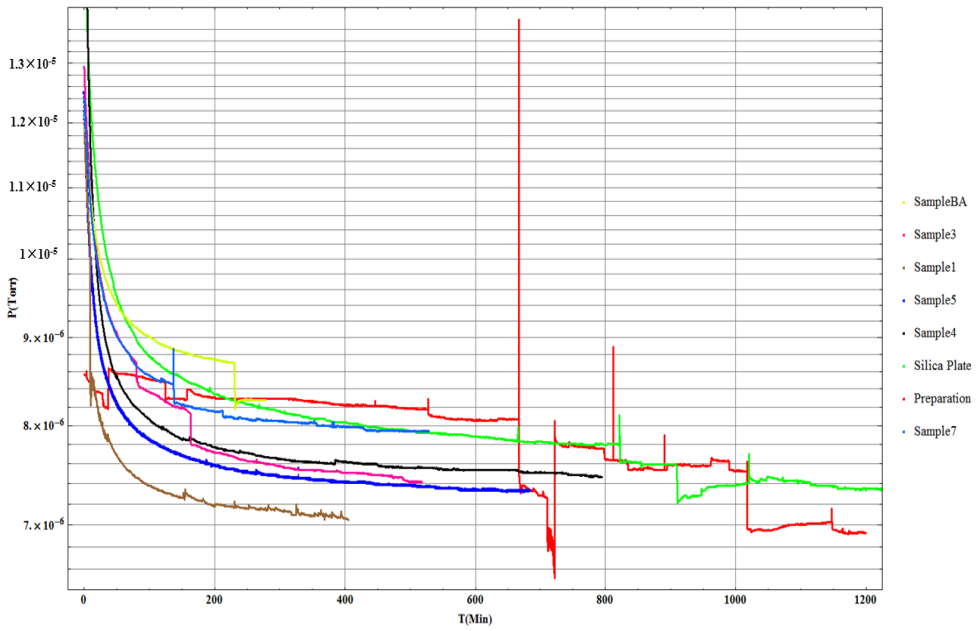

Figure A.5: Time vs Vacuum Pressure History during all runs.

Figure A.5 is representing the vacuum history for all runs. It also gives a rough estimate of run time for each sample. I have drawn vacuum history only for high vacuum gauge. The cause of noise during preparation could be from activities around high vacuum gauge during that data taking.

References:

[1] T. Mibe, *et al*.,"Systematic studies on muonium production in vacuum from laser-ablated silica aerogel (2016A0180)", MLF proposal.
[2] AIM-S-DN40CF: https://shop.edwardsvacuum.com/products/d14662000/view.aspx
[3] http://graphteccorp.com/instruments/gl820/index.html